MICROFLUIDIC PLATFORMS FOR PROTEIN CRYSTALLIZATION AND *IN SITU* X-RAY ANALYSIS

BY

SUDIPTO GUHA

THESIS

Submitted in partial fulfillment of the requirements
for the degree of Master of Science in Chemical Engineering
in the Graduate College of the
University of Illinois at Urbana-Champaign, 2010

Urbana, Illinois

Adviser:

Professor Paul J.A. Kenis

Abstract

Recent efforts associated with the Protein Structure Initiative from the National Institutes of Health (NIH) have eased the bottlenecks associated with protein expression, purification, and crystallization for structural analysis. While strategies have been developed for dealing with each of these challenges in a high throughput fashion, crystal harvesting and mounting for X-ray structure determination is still largely a manual process. During mounting there is a significant potential for damaging fragile protein crystals, both from physical and environmental shock. Microfluidic strategies for protein crystallization have been limited in their application because of a variety of reasons including (i) difficulties in harvesting crystals from chips and (ii) translating results obtained on-chip to a larger scale. The fabrication and operation of an X-ray compatible microfluidic device architecture that allows for on-chip crystallization and *in situ* X-ray analysis of protein crystals while maintaining the advanced fluid handling capabilities of multilayer microfluidics is reported here. The design uses a traditional thin polydimethylsiloxane (PDMS) fluid layer to enable the actuation of pneumatic valves. The traditional glass substrate and thick PDMS control layer are replaced with thin layers of cyclic olefin copolymer (COC). This hybrid COC-PDMS device architecture takes advantage of the low X-ray scattering cross-section of organic polymers such as COC while minimizing the path-length of the more strongly scattering silicon-based PDMS. The device also addresses concerns associated with evaporative losses from the traditional PDMS based devices. X-ray compatible microfluidic chips consisting of arrays of well were implemented using this architecture. The quality of crystals grown on-chip can be screened *in situ* and either standard single-crystal cryogenic analysis or room temperature "single-shot" analysis of many crystals can be used to collect data for protein structure determination. We validated our approach by crystallizing the soluble proteins lysozyme, thaumatin, ribonuclease A, bacterial lyase and bacterial defluorinase on-chip and performing *in situ* X-ray crystallographic analysis.

Acknowledgements

This work would have not been possible without the help and support of a number of people whom I wish to acknowledge here. First and foremost, I would like to thank my advisor Dr. Paul J.A. Kenis for his constant support and encouragement throughout the entire course of the project. I greatly appreciate the fact that he allows all his graduate students to think and work independently on their projects and because of this my experience in graduate school has been a very enriching one so far. Next I would like to acknowledge my lab members, particularly Dr. Sarah Perry who was instrumental in starting this project and helped me tremendously during my initial years in the lab. Further, I would like to thank my co-workers Dr. Amit Desai, Dr. Daria Khovstichenko, Dr. Ashtamurthy Pawate, Josh Tice, Mike Thorson, Sachit Goyal and Ritika Mohan for their help in various parts of my project and providing me invaluable input during my project. Thanks also to the rest of the members of my group for fruitful discussions on my research topic.

My project required a lot of material and input from various other labs, and in this regard I want to acknowledge Dr. Satish Nair and his graduate student Vinayak Agarwal and Dr. Bob Gennis from the Biochemistry department for their help in providing me various proteins to work with. I also wish to thank the beamline staff at LS-CAT (Dr. Joe Brunzelle and Dr. Spencer Anderson), BioCARS (Dr. Zhong Ren) and Dr. Danielle Gray for educating me on the various aspects of X-ray crystallography and helping me set up experiments at the Advanced Photon Source. Also, none of this work would have been possible without funding from NIH.

Last, but not in any way the least, I would like to thank my family, particularly my parents and younger brother for their constant support and encouragement all throughout my life.

To my Parents

Table of Contents

Chapter 1: Introduction *1*

1.1 Protein crystallization **1**

1.2 The Ideal crystallization platform **3**

1.3 Microfluidic platforms for protein crystallization **4**

1.4 *In situ* protein crystallography on microfluidic platforms **6**

1.5 Summary **7**

1.6 Figures **9**

1.7 References **14**

Chapter 2: Material characterization and fabrication of X-ray compatible microfluidic platforms *17*

2.1 Material properties **17**

2.1.1 Scattering and attenuation of X-rays 17

2.1.2 Solvent compatibility and permeability, optical properties 19

2.2 Fabrication of X-ray compatible microfluidic platforms **20**

2.3 Materials and methods **22**

2.3.1 Protein solutions 22

2.3.2 Traditional crystallization experiments 23

2.3.3 X-ray data collection and analysis 23

2.4 Conclusion **24**

2.5 Figures and Tables **25**

2.6 References **31**

Chapter 3: X-ray compatible microfluidic crystallization platforms for in situ protein crystallography *33*

3.1 Single well microfluidic chips for proof-of-concept studies **33**

3.1.1 Design and operation 33

3.1.2 Validation of device architecture with single well microfluidic wells 34

3.2 Microfluidic array chips for screening protein crystallization **35**

3.2.1 Design and operation 35

3.3.2 Screening of crystallization conditions 36

3.3 Microfluidic chips for *in situ* structure determination from multiple crystals **37**

3.4 Conclusion **39**

3.5 Figures and tables **40**

3.6 References **50**

Chapter 4: Concluding remarks *51*

4.1 Summary **51**

4.2 Future directions **51**

4.3 References **52**

Chapter 1

Introduction

Proteins play a central role in biological processes and are the true workhouses of all living systems. They play an important role in material transport, cell-cell signaling, energy storage and transduction, immune response and interaction between intra and extra cellular environment. They are a fundamental component of all living beings, and exist in various forms like enzymes, antibodies and hormones. Proteins consist of one or more chains of amino acids which are linked through peptide bonds and are maintained in distinct 3-dimensional structures. They fold into structural units consisting of alpha helices, beta sheets and other folded shapes with structural integrity being provided by chemical bonding between these structures. They carry out most of the chemical processes and make up a majority of the cellular structures.[1] To understand protein function we need to know their structure and this is the ultimate aim of the work presented here.

1.1 Protein crystallization

Whereas genomics can reveal the sequence of amino acids in a protein, structural biology tells us how that sequence folds up into a particular shape.[2] The different functions of the protein molecule and its interaction with other molecules are determined by its 3-dimensional structure. The human proteome is estimated to contain at least a million proteins, so in order to map out the functionality of all the proteins an efficient, high throughput technological effort is required to determine structural information for all human proteins.[3] The Protein Structure Initiative (PSI) was launched by the National Institute of General Medical Sciences (NIGMS), part of the National Institutes of Health (NIH) in 2000 with the aim of obtaining high resolution structures of 10000 proteins in a decade.[4] To achieve this goal, the PSI also focused on the development of innovative approaches and tools that streamline and speed many steps involved in generating protein structures, and to incorporate these new methods into process pipelines that turn DNA sequence information into protein structures. Figure 1.1 shows the rapid development

achieved by the PSI in solving and depositing structures of proteins. Similar to this, the Membrane Protein Initiative Roadmap has been instrumental in driving research for structure determination of membrane proteins.

Protein structures are considered a treasure trove of information about life's molecular machines. The use of X-ray crystallography and nuclear magnetic resonance spectroscopy reveal structural information which provides insight into how these complex machines operate. Often these insights can help to discover the likely function of an unknown protein, lead to a deeper understanding of how misshaped proteins cause disease, and potentially reveal a path to new drug treatments.[2]

While the success of structural biology efforts has been limited by bottlenecks associated with protein expression,[5-10] purification,[10,11] and crystallization,[12-18] the development of high throughput strategies utilizing robotics[4,13,19-22] and/or microfluidics[14,23-73] have helped to overcome some of these challenges. Automated methods also exist for the screening and collection of X-ray diffraction data from protein crystals.[22,74] Despite this level of automation, the harvesting and mounting of crystals for X-ray analysis remains the only fully manual step in the structural biology pipeline.[19,62,64,67,75]

Once the protein has been expressed and purified satisfactorily, the next and most crucial step to obtaining structural information about the protein is growing diffraction quality crystals. However, methods for predicting protein crystallization conditions *a priori* have do not exist, so obtaining high quality crystals involves searching a vast multidimensional chemical space which could involve screening thousands of different precipitants, buffers, salts etc. in separate crystallization trials.[67,68,76-78] Traditional vapor diffusion[15,16,79-82] and microbatch[21,83,84] methods continue to be the most commonly used crystallization techniques. However for sparse matrix screening a sizeable quantity of protein solution is required which is not always feasible in the initial stages of protein crystallization because of either difficulty in the expression or purification of a hitherto unknown protein. Scalability is also an issue with current platforms. Hence technology that could screen hundreds of conditions using minimal amount of protein solution would significantly benefit the field.

Once optimal crystallization conditions have been identified, traditional methods in X-ray crystallography require manual harvesting of the crystal from the crystallization chamber and mounting of the crystal onto a loop. Handling of crystals can be particularly challenging if the crystals are small and

fragile and can also lead to damage of the crystal due to handling and environmental shock that can occur when the crystal is retrieved from the environs in which it was grown.[33,80] In case of many hard to crystallize proteins, micro crystals can be grown, but mounting and collecting data from such crystals presents a challenge. Advances in synchrotrons have lead to the development of micro beams which can obtain structural information from such crystals, but harvesting and mounting these tiny crystals manually is in extremely challenging. A crystallization platform which enables *in situ* analysis would allow collecting slices of data from many such micro crystals and merging them to get a complete dataset. Removal of this final, manual step of harvesting and ability to perform *in situ* analysis will open up the possibility of getting structural information from recalcitrant protein targets.

1.2 The ideal crystallization platform

Based on the above mentioned issues in the current approach to perform X-ray crystallography on protein crystals, the attributes of an ideal crystallization platform can be enumerated as follows:

1. Ability to screen multiple conditions, in high throughput fashion for protein crystallization
2. Requirement of minimal amount of protein solution for crystallization trials
3. Capability of *in situ* analysis
4. Ability of growing multiple crystals of the same protein for merging datasets

Microfluidics has the capability of manipulating fluids on a very small scale ranging from microliters down to picoliters, and this has been used for a variety of applications ranging from chemical synthesis to biological studies.[85] The ability to control fluid flow at such a small scale makes it an ideal platform for crystallization since microfluidic devices use minimal amounts of protein and precipitant which need to be mixed by free interface diffusion (FID) or counter diffusion in order for crystals to grow. Ease of scaling out of microfluidic systems will enable setting up screens of hundreds of crystallization conditions while maintaining control over the conditions in each individual trial. Traditional microfluidic chips are usually made out of materials which are not suited for *in situ* analysis, which is discussed in further detail in the Chapter 2. To overcome this issue, we use a material which is compatible with *in situ* X-ray analysis and also convenient for fabrication of microfluidic chips. The material selection and subsequent design and fabrication of an X-ray compatible microfluidic device is one of the main focus areas of the research reported in this thesis. As discussed earlier, diffraction quality crystals of some novel proteins have been

challenging to grow, but showers of micro crystals which are individually too small to solve a structure completely have been grown. Since microfluidics offers such precise fluid control and handling at a small, micro crystals of difficult proteins can easily be grown once the crystallization condition is known, and subsequently the protein structure can be obtained by collecting multiple datasets from many crystals and merging them together. In summary, with its small scale, microfluidics addresses the current problems in protein crystallization in two ways: firstly, by allowing experiments to be carried out on novel proteins which are not available in large amounts and secondly, by enabling us to perform experiments which are difficult to implement on a large scale.

1.3 Microfluidic platforms for protein crystallization

In the same way in which integrated circuits brought about many technical advances in the electronics and computation industry, the ability of microfluidics to integrate multiple laboratory functionalities on a single chip significantly impact the field of chemical synthesis and biological studies. This ability of integration of massively parallel operations on a single chip has not only the potential to increase the speed and reliability of many conventional processes, but also bring down the cost of manufacturing and operation due to economies of scale. Microfluidics has been gaining popularity in structural biology, and has shown promise in many related fields ranging from studying protein folding with time resolved studies to growing high quality protein crystals for structure determination. [53,67,86,87]

Microfluidics devices for protein crystallization can be categorized into three main categories, (i) devices with active valves (ii) droplet based devices and (iii) systems based on mimicking well plates, e.g. SlipChip.[78] All these systems deal with nanoliters volumes of protein and precipitant solution but differ in the way of operation and use.

In microfluidic systems of the first type, valves control the fluid flow of the solutions on the device. The most prevalent valves in microfluidics are based on pneumatic actuation and can be broadly classified as (i) actuate-to-open[85,88] (Figure 1.2a) and (ii) actuate-to-close[89] (Figure 1.2b). Typically, the actuation of pneumatic microfluidic valves is based on the actuation of a thin membrane by pressurized air in a control layer that is positioned over a network of microchannels embedded in a fluid layer. Actuate-to-close valves are operated by applying a positive pressure to collapse the membrane over the fluid layer into the fluid channel and thus closing the channel, and need rounded fluid channels for the

membrane to completely stop the flow or drive fluid out of the fluid chamber. This effect is similar to pressing down on a ketchup packet and the ketchup squirting out from the mouth of the packet. When the valves are not actuated, these valves are open, so transporting these chips from the fluid handling station to the X-ray chamber can lead to unwanted mixing between the various chambers. Microfluidic systems based on these valves need external ancillaries to operate the valves and thus are not suitable for portability.

Alternatively, actuate-to-open valves are closed in their rest state. These valves are operated by applying vacuum in the control layer, which causes the thin membrane to deflect upwards, allowing flow or mixing of the fluids in the fluid layer beneath. These valves are closed at rest so devices based on these valves can be transported easily without leading to unwanted mixing. However they require selective reversible bonding of the fluid layer to the substrate so as to allow the multiple actuations of the valves. These valves can be patterned much more densely than the actuate-to-close valves and thus are useful for fabrication of dense microfluidic networks.[85,88] Figure 1.3a shows some of the crystallization platforms which are based on the pneumatic valve networks. These valves have significant potential in high throughput screening applications where portability is desired.

In droplet based methods, a second type of microfluidic platforms that relies on two phase flow, protein crystallization takes place inside aqueous volumes of a mixture of protein and precipitant which are surrounded by an immiscible carrier fluid (e.g. oil) as shown in Figure 1.3b.[26-28,78] The crystallization trials can be conducted in tubes or capillaries made out of plastic or glass. These methods allow for trials to be set up to mimic microbatch and vapor diffusion trials and allow for *in situ* analysis of crystals grown in the case where the capillaries are made out of X-ray transparent materials.[30] Recent advances have also allowed lipidic cubic phase generation on these droplet based devices for carrying out *in meso* crystallization trials.[78,90]

The SlipChip is an example of the third type of microfluidic platform in which the protein and precipitant are loaded into two different wells on different substrates which can slide relative to each other (Figure 1.3c).[43,78,91] The motion of the plates brings the two solutions in contact, thus driving protein crystallization. In these chips, this relative motion of the wells is comparable to the valve actuation in the valve based devices. This method enables exact metering of nanoliters of solution in to the wells on each

of the plates which are then brought into contact. One of the main advantages of this method is the simple operation of these chips, since the operation doesn't need any external ancillary system to set up the actual trial.

1.4 *In situ* protein crystallography on microfluidic platforms

The challenge in implementing *in situ* analysis on a microfluidic chip is finding a material which offers minimum scattering and attenuation from X-rays. Once a suitable material has been identified design and fabrication of a microfluidic chip has to be developed to implement *in situ* analysis on microfluidic platforms. Traditional methods for protein crystallography involve looping the crystal out of the mother liquor and flash freezing it in liquid nitrogen. This prevents formation of ice on the crystal. The looped crystal can be used for cryogenic data collection. While the mother liquor will still be present in most microfluidic systems, addition of cryoprotectant is possible to allow for cryogenic data collection. Additional challenges in development of an *in situ* microfluidic system pertain to device geometry and size so that it can be accommodated on present beamlines setup for X-ray data collection. A chip which can be mounted on the current standardized setup on most synchrotrons would be highly beneficial as it can use the technology currently in place right away.

X-ray capillaries have been traditionally associated with crystallography. These capillaries are not always suited for protein crystallography especially under cryogenic conditions because of their length which can be several centimeters. The long tubes are necessary to obtain the required distance for diffusion to occur and consequently grow many droplets of crystals. However, during cryocooling, not all the drops in the long capillary can be cooled with the narrow cryostream which is only a few millimeters in diameter. The remaining portion of the capillary will still be at room temperature and will act as a heat sink for the cooled part. Therefore, these conventional systems suffer from sub optimal cryocooling and ice formation. Microfluidic systems based on droplets in capillaries or tubes suffer from the same problems and require cutting out the region of interest or harvesting the crystal out of the device in order to collect data. Figure 1.4 illustrates some of the platforms which are based on capillaries that have been developed for *in situ* analysis.

Microfluidic chips for *in situ* analysis require a different choice of material from traditional microfluidics. The majority of microfluidic devices reported in the literature have been fabricated out of

relatively thick layers of polydimethoxysilane (PDMS) and glass, materials which result in significant attenuation of X-rays,[92] thus rendering the devices unsuitable for *in situ* analysis.[24-29,31,32,71,78,93-95] While materials like polyimide (PI), polycarbonate (PC), poly methyl methacrylate (PMMA), polystyrene (PS) and cyclic olefin copolymer (COC) which attenuate X-rays to a lesser extent have been used to make microfluidic devices,[46,60,63,66,96-101] these devices have been limited to single layer devices with little or no integrated fluid handling capabilities (Figure 1.5). Simple counter diffusion and free interface diffusion based microfluidic chips have been fabricated and tested for *in situ* protein crystallography, these devices usually comprise of microchannels molded into a plastic substrate which is X-ray transparent.[53,60,102,103] Figure 1.5 gives examples of various chips which have simple geometries and carry out protein crystallization by either counter diffusion or free interface diffusion. In all these examples, chips have been fabricated from thin layers of an organic based polymer to minimize the scattering and attenuation from X-rays. The main issue with these devices is that they consist of relatively simple networks and are single layered devices that don't have active fluid control which would be necessary for more involved experiments. The few instances in which a multi-layer device was used for protein structure determination, involved punching out the area of interest for further analysis, which is not suited for high throughput crystallography.[53,103,104]

1.5 Summary

Protein crystallization is still very much an art instead of a science. No methods exist for predicting crystallization conditions beforehand and this makes it necessary to set up of thousands of crystallization screening trials before identifying one or more suitable condition. Even after obtaining such a condition, a protein structure is not guaranteed as the crystals grown may not be of high quality or large enough to yield good quality data. Methods to carry out further studies of protein dynamics and interaction have not been fully developed yet. Manual handling of crystals is still needed to harvest them out of the well or plates the trial has been set up in and subsequently loop them so that X-rays can be shot at them for structure determination. Crystals that are fragile and small have the potential to be damaged during this step. Automation of the crystal handling, the only manual step in the current process for protein structure determination, will obviate any human intervention once the trial has been set up.

Microfluidics has the potential to impact the field by facilitating on-chip crystallization and convenient handling of the crystals, followed by *in situ* analysis.

The work described here hopes to address these challenges. In Chapter 2, new protocols for fabrication of a hybrid microfluidic platform fabricated out of COC, which is X-ray transparent, has been described. This platform would allow *in situ* analysis of protein crystals while retaining the functionality and fluid control of a complex microfluidic network on-chip. Integrating this platform with current synchrotron facilities has also been discussed. In Chapter 3 validation of this platform with several proteins is discussed. The data collection strategy for collecting data from multiple crystals and merging them to get a complete dataset is also discussed.

Microfluidic platforms have tremendous potential to address many problems with respect to studying difficult systems in structural biology. The first step to realize this potential is to validate a robust platform that can screen multiple crystallization conditions and allow *in situ* structure determination of novel proteins. Later, this platform can be adapted to study various aspects of dynamic crystallography, including protein folding and kinetics, and interaction with other biomolecules.

1.6 Figures

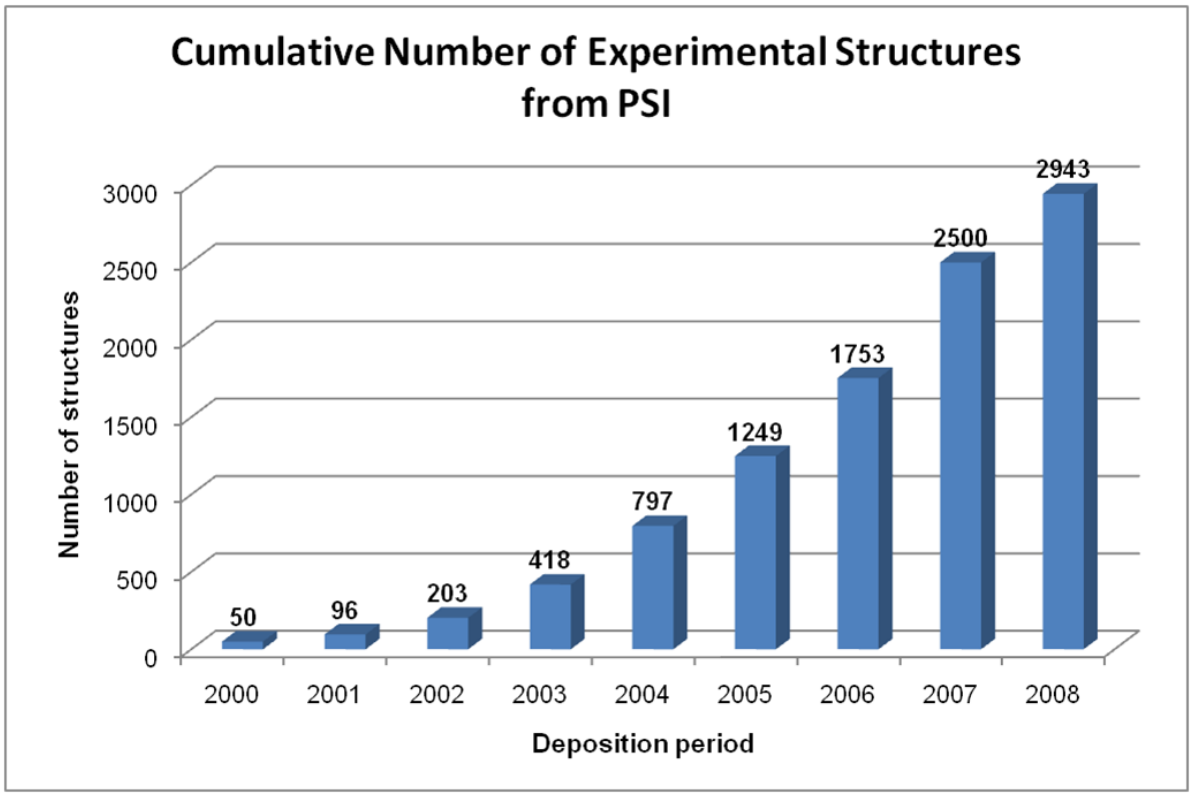

Figure 1.1: Plot showing the rapid progress made by the Protein Structure Initiative (PSI) in terms of protein structures solved, since its inception in 2000. (Figure adapted from Service R.F., 2008).

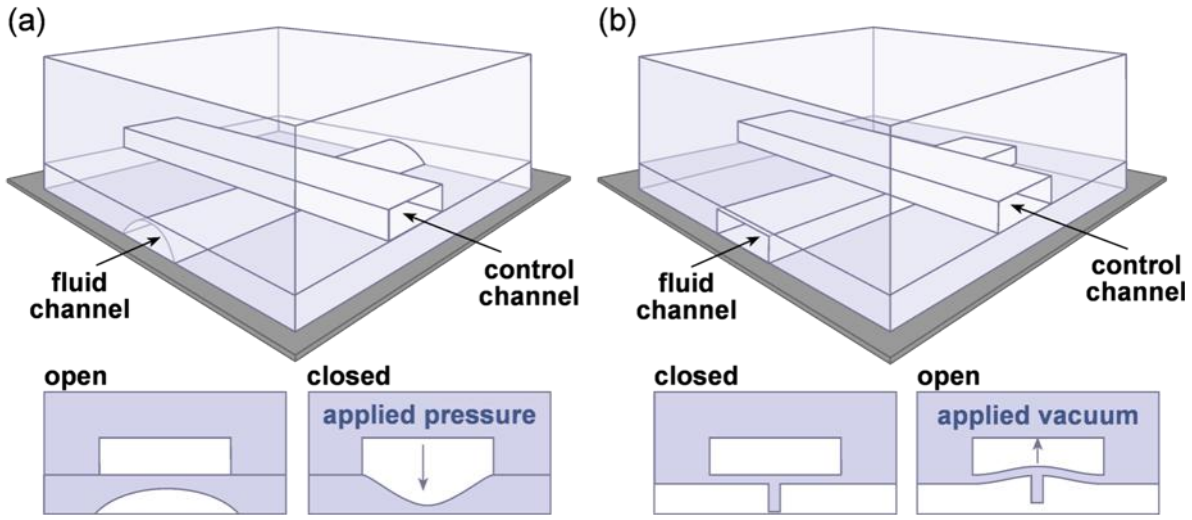

Figure 1.2: Schematic showing operation of microfluidic valves by deflection of a thin membrane by **(a)** positive pressure in an actuate-to-close configuration, or **(b)** negative pressure in an actuate-to-open configuration.

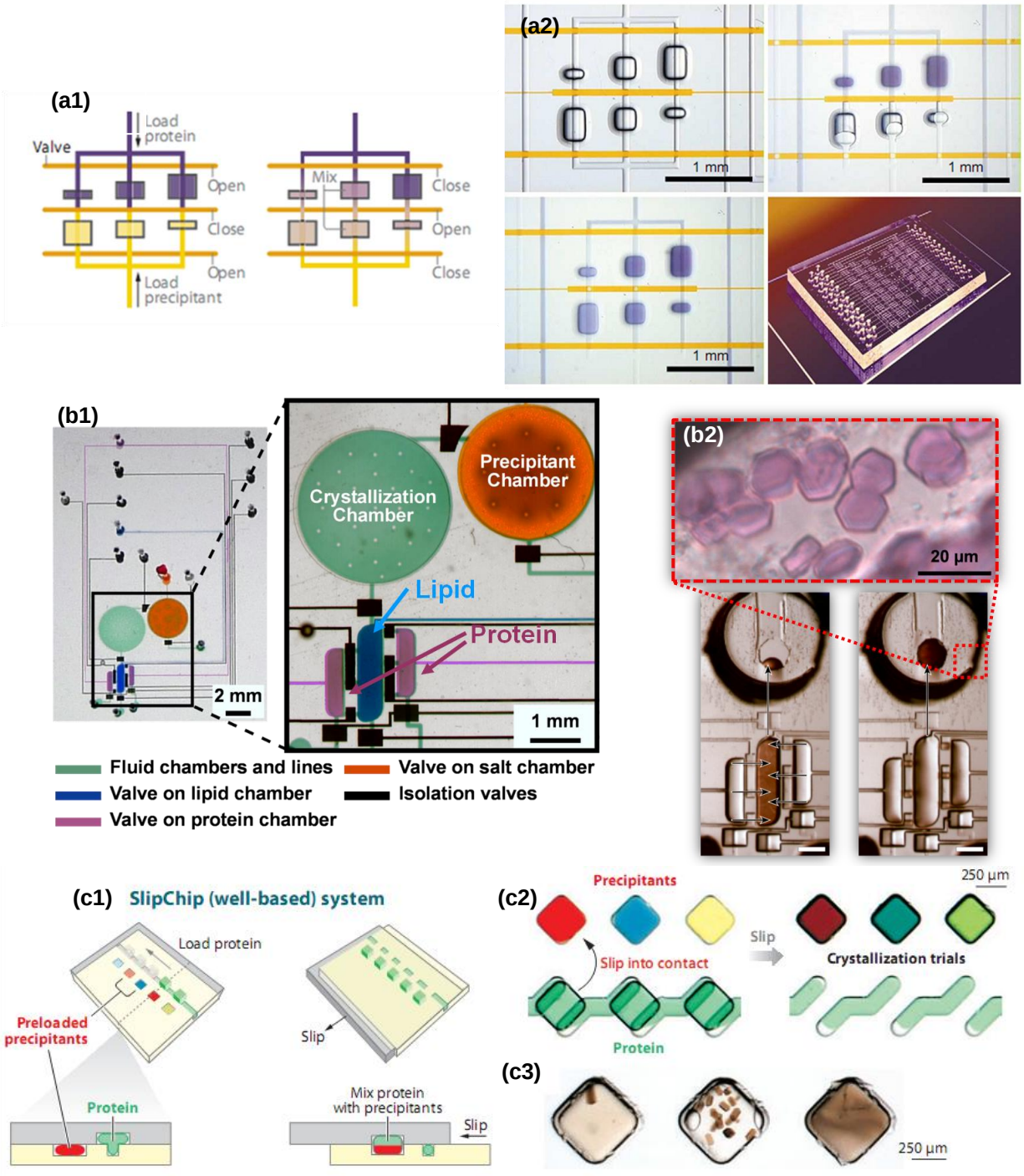

Figure 1.3: Microfluidic chips for protein crystallization (a) Microfluidic chip to implement three different ratios for free interface diffusion assays. (a1) Schematic showing loading of protein and precipitant. (a2) Free interface diffusion on-chip. (b) On-chip generation of lipidic cubic phase for membrane protein crystallization. (b1) Schematic of the chip showing the lipidic cubic phase mixer and the precipitant and crystallization chambers. (b2) Micrograph of the chip with crystals of bacteriorhodopsin grown on-chip. (c) A SlipChip well based system. Schematics showing (c1) the loading of protein and mixing of protein with precipitant on-chip. (c2) Micrograph of loading green food dye (protein) into the chip and bringing it in contact it with colored solutions (precipitants) thus setting up the trial. (c3) Crystals of photosynthetic reaction center grown on the SlipChip. (Figures adapted from Li *et al.,* 2010, Hansen *et al.,* 2003, Perry *et al.,* 2009 and)[14,67,71]

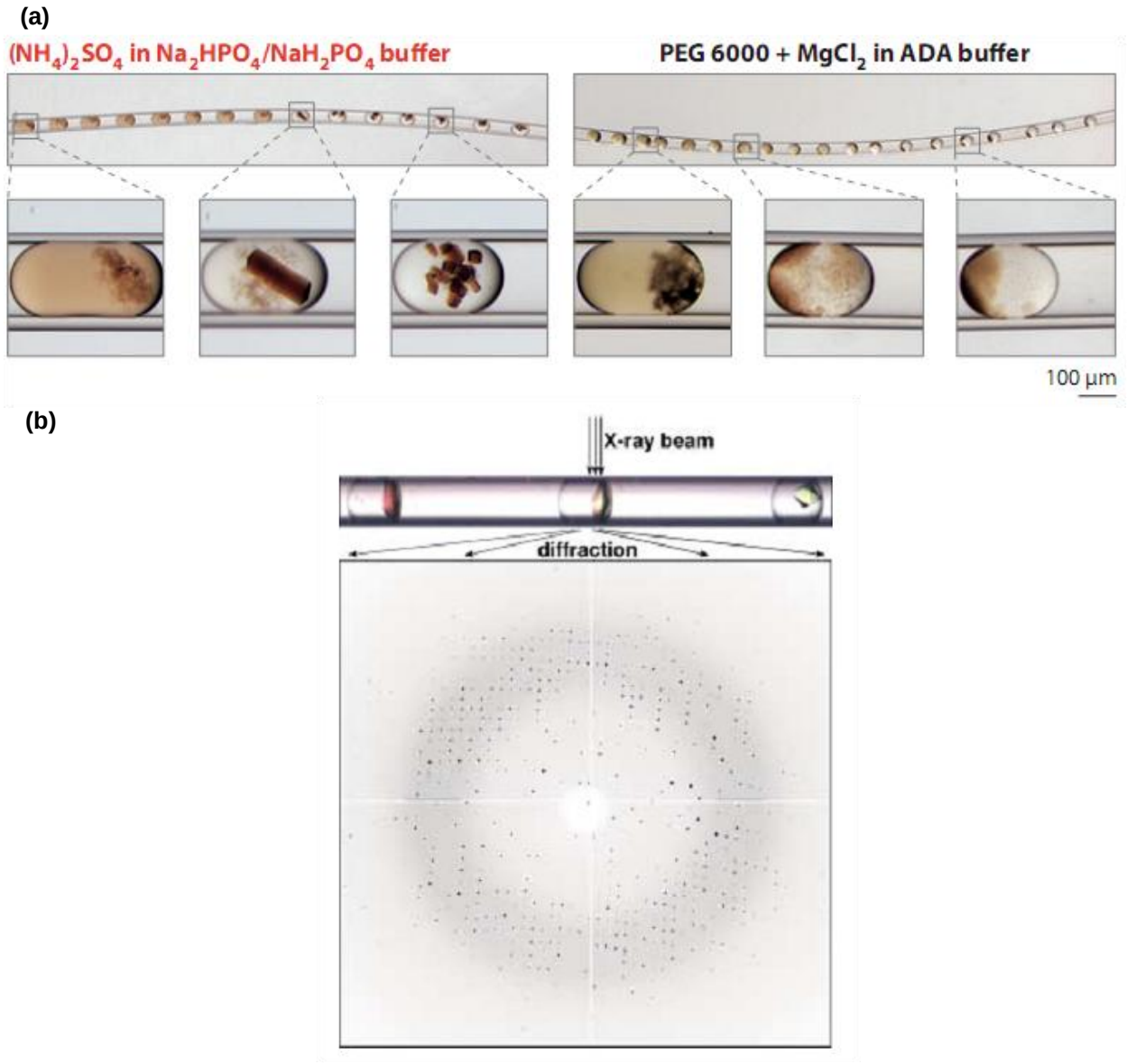

Figure 1.4: (a) Microphotographs of two regions in a Teflon capillary containing droplets of a crystallization trial of photosynthetic reaction center (RC). (b) Diffraction pattern at a resolution of 2.0 A from a thaumatin crystal grown on-chip. (Figures adapted from Li *et al.,* 2010 and Zheng *et al.,* 2004)[14,25]

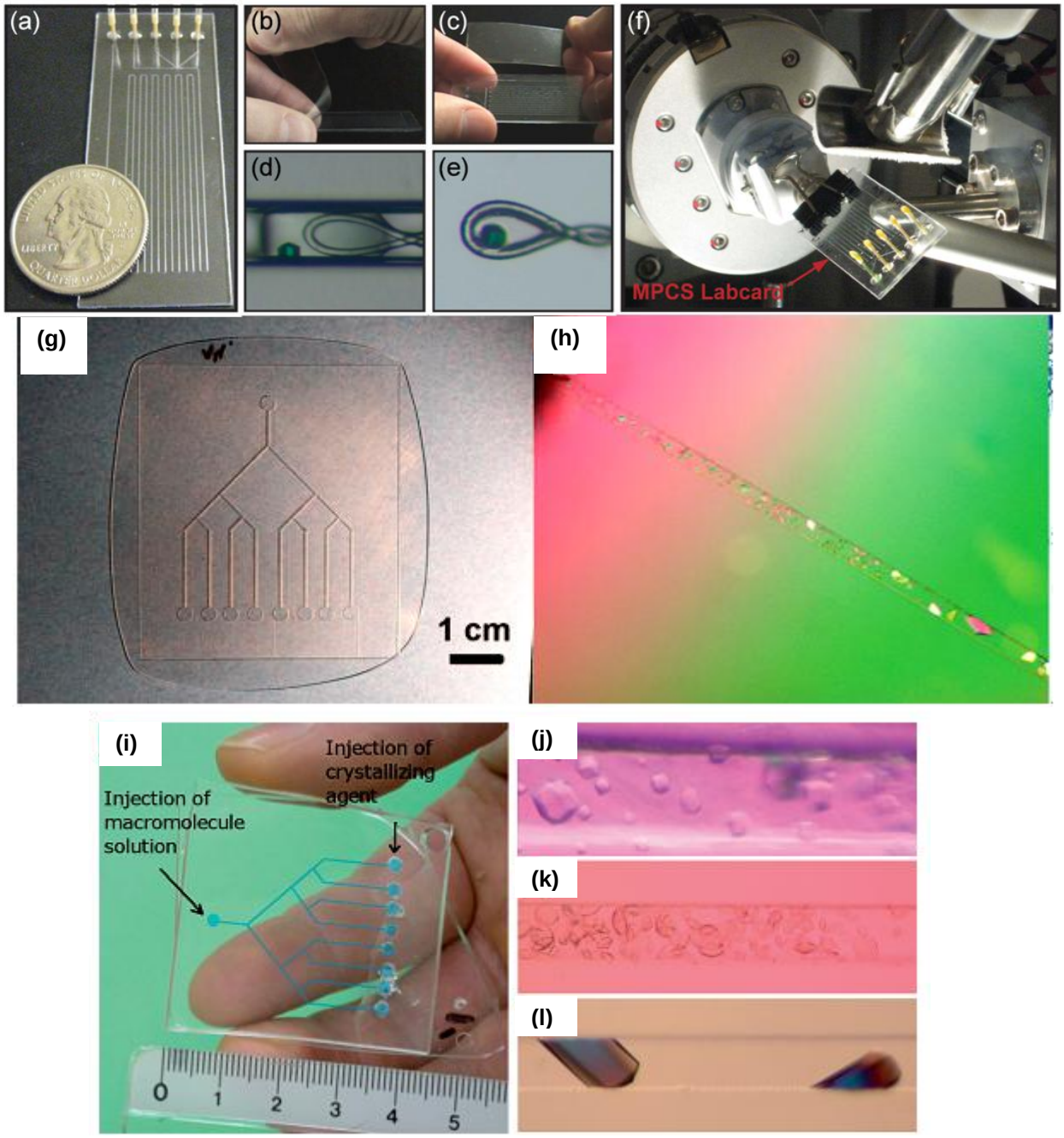

Figure 1.5: (a) A picture of the plastic CrystalCard produced by deCODE Biosystems, combining a microfluidic formulator and a winding storage channel. (b-c) The thin plastic cover being removed from the CrystalCard. (d-e) Optical micrographs of a crystal grown on-chip being harvested with a cryoloop. (f) A picture of the CrystalCard mounted on the goniometer head of an X-ray source for *in situ* analysis. (g) Microfluidic chip made of PMMA by hot embossing. (h) Distribution of crystals of Thaumatin in a microchannel. (i) A chip for biomolecule crystallization by counter diffusion, shown here are eight crystallization channels connected through a dichotomic tree-like network between the inlet for biological sample and the inlets for the crystallization agent. (j-l) Crystals of bovine insulin (j), plant virus (k) and turkey egg white lysozyme (l) grown in the chip shown in (i). (Figures adapted from Gerdts *et al.,* 2008, Sauter *et al.,* 2007 and Dhouib *et al.,* 2009)[40,66,63]

1.7 References

(1) Houghton Mifflin Company: 2005.
(2) Service, R. F. *Science* **2008**, *319*, 1610-1613.
(3) May, M. *Science*, *330*, 689.
(4) Service, R. *Science* **2005**, *307*, 1554-1558.
(5) Hanson, D. K.; Mielke, D. L.; Laible, P. D. In *Current Topics in Membranes, Volume 63*; Volume 63 ed.; DeLucas, L., Ed.; Academic Press: 2009, p 51-82.
(6) Tanabe, M.; Iverson, T. M. In *Current Topics in Membranes, Volume 63*; Volume 63 ed.; DeLucas, L., Ed.; Academic Press: 2009, p 229-267.
(7) Geertsma, E. R.; Groeneveld, M.; Slotboom, D. J.; Poolman, B. *P Natl Acad Sci USA* **2008**, *105*, 5722-5727.
(8) Nollert, P.; Navarro, J.; Landau, E. M. *Method Enzymol* **2002**, *343*, 183-199.
(9) Ostermeier, C.; Michel, H. *Current Opinion in Structural Biology* **1997**, *7*, 697-701.
(10) Lewinson, O.; Lee, A. T.; Rees, D. C. *J Mol Biol* **2008**, *377*, 62-73.
(11) Newby, Z. E. R.; O'Connell, J. D.; Gruswitz, F.; Hays, F. A.; Harries, W. E. C.; Harwood, I. M.; Ho, J. D.; Lee, J. K.; Savage, D. F.; Miercke, L. J. W.; Stroud, R. M. **2009**, *4*, 619-637.
(12) Durbin, S. D.; Feher, G. *Annu Rev Phys Chem* **1996**, *47*, 171-204.
(13) Stevens, R. C. *Current Opinion in Structural Biology* **2000**, *10*, 558-563.
(14) Li, L.; Ismagilov, R. F. *Ann Rev Biophys* **2010**.
(15) McPherson, A. In *Current Topics in Membranes, Volume 63*; Volume 63 ed.; DeLucas, L., Ed.; Academic Press: 2009, p 5-23.
(16) Gabrielsen, M.; Gardiner, A. T.; Fromme, P.; Cogdell, R. J. In *Current Topics in Membranes, Volume 63*; Volume 63 ed.; DeLucas, L., Ed.; Academic Press: 2009, p 127-149.
(17) Page, R. In *Methods in Molecular Biology: Structural Proteomics - High Throughput Methods*; Kobe, B., Guss, M., Huber, T., Eds.; Humana Press: Totowa, NJ, 2008; Vol. 426, p 345-362.
(18) Dauter, Z.; Lamzin, V. S.; Wilson, K. S. *Current Opinion in Structural Biology* **1997**, *7*, 681-688.
(19) Cherezov, V.; Peddi, A.; Muthusubramaniam, L.; Zheng, Y. F.; Caffrey, M. *Acta Crystallogr D* **2004**, *60*, 1795-1807.
(20) Iacovache, I.; Biasini, M.; Kowal, J.; Kukulski, W.; Chami, M.; van der Goot, F. G.; Engel, A.; Rémigy, H.-W. *Journal of Structural Biology*, *In Press, Corrected Proof*.
(21) Chayen, N. E.; Stewart, P. D. S.; Maeder, D. L.; Blow, D. M. *J Appl Crystallogr* **1990**, *23*, 297-302.
(22) Fogg, M. J.; Wilkinson, A. J. *Biochemical Society Transactions* **2008**, *036*, 771-775.
(23) Li, L.; Du, W.; Ismagilov, R. F. *J Am Chem Soc* **2009**.
(24) Zheng, B.; Roach, L. S.; Ismagilov, R. F. *J Am Chem Soc* **2003**, *125*, 11170-11171.
(25) Zheng, B.; Tice, J. D.; Ismagilov, R. F. *Adv Mater* **2004**, *16*, 1365-1368.
(26) Zheng, B.; Tice, J. D.; Ismagilov, R. F. *Anal Chem* **2004**, *76*, 4977-4982.
(27) Zheng, B.; Tice, J. D.; Roach, L. S.; Ismagilov, R. F. *Angew Chem Int Edit* **2004**, *43*, 2508-2511.
(28) Zheng, B.; Gerdts, C. J.; Ismagilov, R. F. *Current Opinion in Structural Biology* **2005**, *15*, 548-555.
(29) Zheng, B.; Ismagilov, R. F. *Angew Chem Int Edit* **2005**, *44*, 2520-2523.
(30) Yadav, M. K.; Gerdts, C. J.; Sanishvili, R.; Smith, W. W.; Roach, L. S.; Ismagilov, R. F.; Kuhn, P.; Stevens, R. C. *J Appl Crystallogr* **2005**, *38*, 900-905.
(31) Chen, D. L.; Gerdts, C. J.; Ismagilov, R. F. *J Am Chem Soc* **2005**, *127*, 9672-9673.
(32) Chen, D. L. L.; Ismagilov, R. F. *Curr Opin Chem Biol* **2006**, *10*, 226-231.
(33) Gerdts, C. J.; Tereshko, V.; Yadav, M. K.; Dementieva, I.; Collart, F.; Joachimiak, A.; Stevens, R. C.; Kuhn, P.; Kossiakoff, A.; Ismagilov, R. F. *Angew Chem Int Edit* **2006**, *45*, 8156-8160.
(34) Li, L.; Mustafi, D.; Fu, Q.; Tereshko, V.; Chen, D. L. L.; Tice, J. D.; Ismagilov, R. F. *P Natl Acad Sci USA* **2006**, *103*, 19243-19248.
(35) Song, H.; Chen, D. L.; Ismagilov, R. F. *Angew Chem Int Edit* **2006**, *45*, 7336-7356.
(36) Chen, D. L. L.; Li, L.; Reyes, S.; Adamson, D. N.; Ismagilov, R. F. *Langmuir* **2007**, *23*, 2255-2260.
(37) Laval, P.; Salmon, J. B.; Joanicot, M. *J Cryst Growth* **2007**, *303*, 622-628.
(38) Dombrowski, R. D.; Litster, J. D.; Wagner, N. J.; He, Y. *Chem Eng Sci* **2007**, *62*, 4802-4810.

(39) Maki, S.; Murai, R.; Yoshikawa, H. Y.; Kitatani, T.; Nakata, S.; Kawahara, H.; Hasenaka, H.; Kobayashi, A.; Okada, S.; Sugiyama, S.; Adachi, H.; Matsumura, H.; Takano, K.; Murakami, S.; Inoue, T.; Sasaki, T.; Mori, Y. *J Synchrotron Radiat* **2008**, *15*, 269-272.
(40) Gerdts, C. J.; Elliott, M.; Lovell, S.; Mixon, M. B.; Napuli, A. J.; Staker, B. L.; Nollert, P.; Stewart, L. *Acta Crystallographica Section D* **2008**, *64*, 1116-1122.
(41) Salmon, J.-B.; Leng, J. *Comptes Rendus Chimie Matière molle et chimie : un mélange fructueux - Soft matter and chemistry: a fruitful melting-pot* **2009**, *12*, 258-269.
(42) Kreutz, J. E.; Li, L.; Roach, L. S.; Hatakeyama, T.; Ismagilov, R. F. *J Am Chem Soc* **2009**, *131*, 6042-6043.
(43) Du, W.; Li, L.; Nichols, K. P.; Ismagilov, R. F. *Lab Chip* **2009**, *9*, 2286-2292.
(44) Pang, Y.; Liu, J.; Li, H.; Lin, J. *Science in China Series B: Chemistry* **2009**, *52*, 1014-1020.
(45) Luft, J. R.; Rak, D. M.; DeTitta, G. T. *J Cryst Growth* **1999**, *196*, 450-455.
(46) Steinert, C. P.; Mueller-Dieckmann, J.; Weiss, M.; Roessle, M.; Zengerle, R.; Koltay, P. In *Future Generation Communication and Networking* 2007, p 561-564.
(47) Zhou, X.; Lau, L.; Lam, W. W. L.; Au, S. W. N.; Zheng, B. *Anal. Chem.* **2007**.
(48) Lounaci, M.; Rigolet, P.; Casquillas, G. V.; Huang, H. W.; Chen, Y. *Microelectron Eng* **2006**, *83*, 1673-1676.
(49) Lounaci, M.; Rigolet, P.; Abraham, C.; Le Berre, M.; Chen, Y. *Microelectron Eng* **2007**, *84*, 1758-1761.
(50) Korczynska, J.; Hu, T. C.; Smith, D. K.; Jenkins, J.; Lewis, R.; Edwards, T.; Brzozowski, A. M. *Acta Crystallogr D* **2007**, *63*, 1009-1015.
(51) Shim, J. U.; Cristobal, G.; Link, D. R.; Thorsen, T.; Fraden, S. *Cryst Growth Des* **2007**, *7*, 2192-2194.
(52) Shim, J. U.; Cristobal, G.; Link, D. R.; Thorsen, T.; Jia, Y.; Piattelli, K.; Fraden, S. *J Am Chem Soc* **2007**, *129*, 8825-8835.
(53) Hansen, C. L.; Classen, S.; Berger, J. M.; Quake, S. R. *J Am Chem Soc* **2006**, *128*, 3142-3143.
(54) Lau, B. T. C.; Baitz, C. A.; Dong, X. P.; Hansen, C. L. *J Am Chem Soc* **2007**, *129*, 454-455.
(55) Lopez-Jaramillo, F. J.; Garcia-Ruiz, J. M.; Gavira, J. A.; Otalora, F. *J Appl Crystallogr* **2001**, *34*, 365-370.
(56) Garcia-Ruiz, J. M.; Otalora, F.; Novella, M. L.; Gavira, J. A.; Sauter, C.; Vidal, O. *J Cryst Growth* **2001**, *232*, 149-155.
(57) Garcia-Ruiz, J. M.; Gonzalez-Ramirez, L. A.; Gavira, J. A.; Otalora, F. *Acta Crystallogr D* **2002**, *58*, 1638-1642.
(58) Gavira, J. A.; Toh, D.; Lopez-Jaramillo, J.; Garcia-Ruiz, J. M.; Ng, J. D. *Acta Crystallogr D* **2002**, *58*, 1147-1154.
(59) Bolanos-Garcia, V. M. *J Cryst Growth* **2003**, *253*, 517-523.
(60) Ng, J. D.; Clark, P. J.; Stevens, R. C.; Kuhn, P. *Acta Crystallographica Section D* **2008**, *64*, 189-197.
(61) Ng, J. D.; Garcia-Ruiz, J. M.; Gavira-Gallardo, J. A.; Wells, M.; Jenkins, G. US, 2006.
(62) Ng, J. D.; Gavira, J. A.; Garcia-Ruiz, J. M. *Journal of Structural Biology* **2003**, *142*, 218-231.
(63) Dhouib, K.; Malek, C. K.; Pfleging, W.; Gauthier-Manuel, B.; Duffait, R.; Thuillier, G.; Ferrigno, R.; Jacquamet, L.; Ohana, J.; Ferrer, J.-L.; Theobald-Dietrich, A.; Giege, R.; Lorber, B.; Sauter, C. *Lab Chip* **2009**, *9*, 1412-1421.
(64) Sugahara, M.; Kageyama, Y.; Kunishima, N. *J Appl Crystallogr* **2009**, *42*, 129-133.
(65) Sauter, C.; Otalora, F.; Gavira, J. A.; Vidal, O.; Giege, R.; Garcia-Ruiz, J. M. *Acta Crystallogr D* **2001**, *57*, 1119-1126.
(66) Sauter, C.; Dhouib, K.; Lorber, B. *Crystal Growth and Design* **2007**, *7*, 2247-2250.
(67) Hansen, C.; Quake, S. R. *Current Opinion in Structural Biology* **2003**, *13*, 538-544.
(68) Hansen, C. L.; Skordalakes, E.; Berger, J. M.; Quake, S. R. *P Natl Acad Sci USA* **2002**, *99*, 16531-16536.
(69) Kothe, M.; Kohls, D.; Low, S.; Coli, R.; Cheng, A. C.; Jacques, S. L.; Johnson, T. L.; Lewis, C.; Loh, C.; Nonomiya, J.; Sheils, A. L.; Verdries, K. A.; Wynn, T. A.; Kuhn, C.; Ding, Y. H. *Biochemistry-Us* **2007**, *46*, 5960-5971.
(70) Sugahara, M.; Asada, Y.; Morikawa, Y.; Kageyama, Y.; Kunishima, N. *Acta Crystallogr D* **2008**, *64*, 686-695.

(71) Perry, S. L.; Roberts, G. W.; Tice, J. D.; Gennis, R. B.; Kenis, P. J. A. *Cryst Growth Des* **2009**, *9*, 2566-2569.
(72) Li, L.; Fu, Q.; Kors, C.; Stewart, L.; Nollert, P.; Laible, P.; Ismagilov, R. *Microfluid Nanofluid* **2009**, *8*, 789-798.
(73) Li, G.; Chen, Q.; Li, J.; Hu, X.; Zhao, J. *Anal Chem* **2010**, *82*, 4362-4369.
(74) Cherezov, V.; Hanson, M. A.; Griffith, M. T.; Hilgart, M. C.; Sanishvili, R.; Nagarajan, V.; Stepanov, S.; Fischetti, R. F.; Kuhn, P.; Stevens, R. C. *Journal of The Royal Society Interface* **2009**, *6*, S587-S597.
(75) van der Woerd, M.; Ferree, D.; Pusey, M. *Journal of Structural Biology* **2003**, *142*, 180-187.
(76) Talreja, S.; Perry, S. L.; Guha, S.; Bhamidi, V.; Zukoski, C. F.; Kenis, P. J. A. *The Journal of Physical Chemistry B* **2010**, *114*, 4432-4441.
(77) Chayen, N. E. *Current Opinion in Structural Biology* **2004**, *14*, 577-583.
(78) Li, L.; Ismagilov, R. F. *Ann Rev Biophys* **2010**, *39*.
(79) Chayen, N. E. *Acta Crystallogr D* **1998**, *54*, 8-15.
(80) McPherson, A. *Crystallization of Biological Macromolecules*; CSHL Press, 1999.
(81) Ng, J. D.; Stevens, R. C.; Kuhn, P. In *Methods in Molecular Biology: Structural Proteomics - High Throughput Methods*; Kobe, B., Guss, M., Huber, T., Eds.; Humana Press: Totowa, NJ, 2008; Vol. 426, p 363-375.
(82) Johansson, L. C.; Wöhri, A. B.; Katona, G.; Engström, S.; Neutze, R. *Current Opinion in Structural Biology Membranes / Engineering and design* **2009**, *19*, 372-378.
(83) Chayen, N. E.; Stewart, P. D. S.; Blow, D. M. *J Cryst Growth* **1992**, *122*, 176-180.
(84) Research, H. *Crystal Growth Techniques*, 2001.
(85) Schudel, B. R.; Choi, C. J.; Cunningham, B. T.; Kenis, P. J. A. *Lab Chip* **2009**, *9*, 1676-1680.
(86) Hansen, C. L.; Quake, S. R.; Berger, J. M.; California Institute of Technology: US, 2007.
(87) Quake, S. R.; Hansen, C. L.; California Institute of Technology: US, 2006.
(88) Grover, W. H.; Skelley, A. M.; Liu, C. N.; Lagally, E. T.; Mathies, R. A. *Sensor Actuat B-Chem* **2003**, *89*, 315-323.
(89) Unger, M. A.; Chou, H. P.; Thorsen, T.; Scherer, A.; Quake, S. R. *Science* **2000**, *288*, 113-116.
(90) Li, L.; Fu, Q.; Kors, C.; Stewart, L.; Nollert, P.; Laible, P.; Ismagilov, R. *Microfluid Nanofluid* **2010**

(91) Li, L.; Du, W.; Ismagilov, R. *J Am Chem Soc* **2009**.
(92) Greaves, E. D.; Manz, A. *Lab Chip* **2005**, *5*, 382-391.
(93) Chen, D.; Du, W.; Liu, Y.; Liu, W.; Kuznetsov, A.; Mendez, F. E.; Philipson, L. H.; Ismagilov, R. F. *Proceedings of the National Academy of Sciences* **2008**, *105*, 16843-16848.
(94) Ismagilov, R. F.; Kenis, P. J. A.; Whitesides, G. H.; Rosmarin, D.; President and Fellows of Harvard College: US, 2005.
(95) Ismagilov, R. F.; Rosmarin, D.; Kenis, P. J. A.; Chiu, D. T.; Zhang, W.; Stone, H. A.; Whitesides, G. M. *Anal Chem* **2001**, *73*, 4682-4687.
(96) Narasimhan, J.; Papautsky, I. *J Micromech Microeng* **2004**, *14*, 96-103.
(97) Steigert, J.; et al. *J Micromech Microeng* **2007**, *17*, 333.
(98) Mehta, G.; Lee, J.; Cha, W.; Tung, Y. C.; Linderman, J. J.; Takayama, S. *Anal Chem* **2009**, *81*, 3714-3722.
(99) Becker, H.; Heim, U. *Sensors and Actuators a-Physical* **2000**, *83*, 130-135.
(100) Becker, H.; Locascio, L. E. *Talanta* **2002**, *56*, 267-287.
(101) Guber, A. E.; Heckele, M.; Herrmann, D.; Muslija, A.; Saile, V.; Eichhorn, L.; Gietzelt, T.; Hoffmann, W.; Hauser, P. C.; Tanyanyiwa, J.; Gerlach, A.; Gottschlich, N.; Knebel, G. *Chemical Engineering Journal* **2004**, *101*, 447-453.
(102) Dhouib, K.; Malek, C. K.; Pfleging, W.; Gauthier-Manuel, B.; Duffait, R.; Thuillier, G.; Ferrigno, R.; Jacquamet, L.; Ohana, J.; Ferrer, J. L.; Theobald-Dietrich, A.; Giege, R.; Lorber, B.; Sauter, C. *Lab Chip* **2009**, *9*, 1412-1421.
(103) Anderson, M. J.; DeLaBarre, B.; Raghunathan, A.; Palsson, B. O.; Brunger, A. T.; Quake, S. R. *Biochemistry-Us* **2007**, *46*, 5722-5731.
(104) Anderson, M. J.; Hansen, C. L.; Quake, S. R. *P Natl Acad Sci USA* **2006**, *103*, 16746-16751.

Chapter 2

Material characterization and fabrication of X-ray compatible microfluidic platforms

The material selection criteria and the fabrication of an X-ray compatible microfluidic device architecture is described in this chapter. The device consists of pneumatic valves fabricated out of thin polydimethylsiloxane (PDMS) membranes for active fluid control. The rest of the structural components of the microfluidic device are fabricated out of cyclic olefin copolymer (COC), which has a low X-ray scattering cross section, compared to PDMS. Thus, a combination of a low X-ray scattering material and a thin membrane of high X-ray scattering material make the device X-ray transparent.

2.1 Material properties

2.1.1 Scattering and attenuation of X-rays

In selection of materials for an X-ray transparent microfluidic device for use in protein crystallography three main considerations with respect to the interaction between materials and X-rays have to be taken into account: (i) attenuation and (ii) scattering of X-rays passing through device materials, and (iii) the strength of the diffraction signal pattern resulting from a crystal. Attenuation results from the absorption of photons into the material, thereby decreasing the intensity of both the incident X-ray beam and the resultant signal. Scattering is an elastic redirection of photons based on the internal structure of the material and can affect the signal-to-noise ratio. Both attenuation and scattering are a function of the thickness of the material through which the X-rays have to penetrate. The strength of the diffraction signal from a crystal is related to not only the degree of order within the crystal, but also the packing density and size of the crystal.[1-5]

Attenuation can be calculated for a particular energy based on the exponential decay in intensity of a narrow beam of monochromatic photons from an incident intensity I_0 as it passes through a material of thickness x with a linear attenuation coefficient μ.[6,7]

$$I = I_0 \exp(-\mu x) \tag{1}$$

Attenuation coefficients have been well studied and documented for elemental materials.[6] For a compound containing multiple elements, a linear attenuation coefficient can be calculated based on the sum of the contribution to attenuation from each of the individual elements i, weighted based on their mass fraction w_i.

$$\mu = \sum \mu_i w_i \tag{2}$$

Table 2.1 lists the atomic mass fractional compositions of various materials commonly used in fabrication of microfluidic devices and Figure 2.1a shows calculated values for the linear attenuation coefficient (using Eq. 1 and 2) for SiO_2, PDMS, and COC as a function of photon energy. As can be seen in Figure 2.1a, the attenuation coefficient decreases significantly with increasing photon energy. Soft X-rays (lower energy) attenuate much more strongly than do harder X-rays (higher energy), thus the energy of X-rays used for an experiment can have a significant effect on the signal observed from a device.

Using values for the attenuation coefficient for X-rays with a wavelength of 1Å (12.4 keV), the transmission factor I/I_0 can then be calculated as a function of material thickness using Eq. 1. A plot of I/I_0 is shown in Figure 2.1b for PDMS and COC. Because crystallography experiments commonly involve sample rotation, variations in path length as a function of the incident angle also need to be taken into account.

Several interesting observations can be made from the data presented in Table 2.1 and Figure 2.1. PDMS and PMMA have very similar densities; however the linear attenuation coefficient for PDMS is significantly higher. This difference arises from the silicon content in PDMS. Heavier atoms present a larger cross-section for interacting with photons and will thus cause a larger degree of attenuation. The density of a material also plays a role in the degree of attenuation observed, with higher density materials increasing the number of atoms which can interact with a photon for a given path length, though this effect is less significant than the effect of elemental composition.

Knowing the attenuation coefficient for various materials, an expression for the attenuation through a series of different films j can be calculated based on Eq. (1) as.

$$I = I_0 \exp\left(-\sum \mu_j x_j\right) \tag{3}$$

A typical device used here will have an X-ray path length of 145 µm of COC and 20 µm of PDMS (50 µm COC substrate, 20 µm PDMS membrane, 75 µm COC control layer). Figure 2.1d shows a plot of transmission factor I/I_0 as a function of photon energy for this device geometry. A transmission factor of around 0.7 is observed for the standard energy of 12.4 keV (corresponding to a wavelength of 1 Å).

In addition to attenuation, background scatter from the device materials can also decrease the intensity of the signal observed. Scattering is a result of the internal structure of a material and thus the characteristic length-scale of this internal geometry defines the location of a scatter ring. An analysis of both PDMS and COC shows that these materials produce a characteristic scattering pattern, as described in Figure 2.2. Scatter from both PDMS and COC occurs at relatively low angles of q-spacing or areas of low resolution diffraction; $q \approx 0.161$ Å^{-1} (7.5 Å) for PDMS and $q \approx 0.232$ Å^{-1} (5.2 Å) for COC. A comparison of the scatter from different thicknesses of COC shows that a roughly linear relationship exists between scattering intensity and sample thickness.

2.1.2 Solvent compatibility and permeability, optical properties

The next material selection criteria for a X-ray compatible microfluidic device is related to the the properties of the solvents used for crystallizing the proteins. Obtaining the optimal crystallization condition for a given protein requires the exploration of a vast chemical space consisting of various precipitants, salts, buffers and detergents.[8] One of the main requirements for a screening and crystallization platform would be compatibility with as many of these crystallization screening components as possible. COC is known to have excellent resistance to a host of non-polar organic solvents and aqueous solvents.[9,10]

One of the major issues with traditional PDMS based microfluidics is the absorption and loss of water and aqueous solutions through the PDMS material.[11] PDMS is also gas permeable which may affect the equilibrium of the crystallization trial set up in a microfluidic device. Crystallization trials are sensitive to protein concentration, so loss of water through the walls of the device implies that the correct crystallization condition will not be maintained throughout the period of the trial. COC has a significantly lower water and gas transmission rate than PDMS which makes it a better candidate for fabricating microfluidic devices where solvent permeability must be kept to a minimum.[10,11] Table 2.2 illustrates that most thermoplastic polymers have significantly lower transmission rates of water and gas than PDMS.

PDMS-based microfluidic devices have an advantage of being optically transparent, which is useful in the visualization of trials set up on a chip. In a hybrid device made out of PDMS and another material, maintaining optical transparency would mean ensuring that the other component is transparent as well. COC is known to have excellent optical clarity, so visualization of on-chip phenomena made out of these hybrid devices will not be an issue.[12]

2.2 Fabrication of X-ray compatible microfluidic platforms

The hybrid microfluidic chips consist of a thin PDMS fluid layer bonded to a COC control layer and a flat COC substrate. Each of these layers was fabricated separately, and then the layers were aligned and bonded. The masks for photolithography needed to make silicon masters for the different layers were designed in Macromedia Freehand MX™ and printed on a 5080 dpi transparency.

The control layer was fabricated out of COC via hot embossing against a robust epoxy mold (Figure 2.3a). To fabricate the epoxy mold, a master for the control layer was created on a silicon wafer with SU-8-25 using standard photolithography, which in turn is replicated onto a PDMS (General Electric RTV 650) negative mold. [13,14] High temperature epoxy resin (Conapoxy FR 1080, 83:100 hardener: epoxy, by mass) was poured on the PDMS negative mold and cured on a hot plate at 120°C for 4 hours to yield the epoxy master. [11,15,16] Care had to be taken to ensure that the hot plate is perfectly flat, otherwise the resulting gradient on the epoxy master will make it difficult to replicate features via hot embossing. To ensure the flatness, the hot plate is leveled using a plumb line and aluminum weights are kept on the PDMS molds while the epoxy is being cured to ensure that the PDMS doesn't warp when heated. Two grades of COC film (5013 and 6013, 2 and 4mils, TOPAS™ Advanced Polymers Inc) were patterned with this epoxy master by hot embossing (Carver hot press, model 3851-0) at 175°C (T_g+50°C), where T_g is the glass transition temperature of COC. The COC sheets were loaded into the hot press in contact with the epoxy master with a glass side for backing on the opposite side of the epoxy. The epoxy master and the glass slide were supported by blocks of flat PDMS to accommodate some surface irregularities in the epoxy master which would otherwise shatter the epoxy master under pressure. The assembly was brought to the temperature of 175°C, maintained there for 5 minutes and then cooled down to 75°C. The assembly was carefully removed from the hot press and the COC control layer is peeled off the epoxy master. The epoxy master can be reused to hot emboss more COC sheets. For fabricating the

flat substrates, COC sheets of the desired thickness were placed between a stack of glass slides and the same hot pressing scheme described above is followed.

The flexible fluid layer was made out of PDMS (15:1, cross-linker : monomer) using standard soft lithographic procedures previously reported.[13,14] Inlets for the fluid and control layer were drilled using a 750 µm drill bit. Scotch tape (3M) is used to protect the layers from damage and dust during drilling.

The COC control layer was then chemically bonded to the thin PDMS fluid layer. Since COC expands during the entire hot embossing process, the dimensions of the fluid layer were scaled up by an expansion factor of 0.015 to ensure that the features aligned perfectly. Preliminary devices with simple architecture and no valves were bonded using an oxygen plasma treatment while array chips with a dense network of valves utilized cross-linking between an epoxy-terminated silane on the surface of the control layer and an amine-terminated silane on the surface of the fluid layer.[17] To achieve this epoxy-amine bond, a 60 second oxygen plasma treatment was used to activate the PDMS and COC surfaces with –OH groups for the formation of a silane bond. Then, the COC control layer was immersed in a 1% (v/v) solution of 3-glycidoxypropyltrimethoxysilane (GPTMS, Sigma Aldrich) and the PDMS fluid layer was immersed in a 1% (v/v) solution of 3-aminopropyltrimethoxysilane (APTMS, Sigma Aldrich) for 20 minutes. After rinsing with DI water and blowing dry with nitrogen gas the two layers were aligned and brought into contact (Figure 2.4). A strong bond forms almost immediately and the structure was allowed to cure for 1 hour at room temperature to reinforce the bond.[17] Since the epoxy amine bonding is instantaneous, the devices have to be aligned in one attempt (*i.e.* contacting the two surfaces once), else the misaligned control and fluid layers brought become partially bonded after which, the two surfaces cannot be taken apart to realign the device. Devices with actuate-to-open valves do not need to be bonded to the COC substrate.[18,19]

Scanning electron microscopy (Hitachi S-4800 High Resolution SEM) was used to visualize the quality of pattern transfer between the SU-8-25 on silicon master, the resulting inverse PDMS master, the epoxy master for hot embossing, and the final COC structure. Scanning electron micrographs in Figures 2.5 and 2.6, indicate high fidelity pattern transfer across all four surfaces, where channels as small as 50 µm wide have been embossed onto the COC control layer.

2.3 Materials and methods

2.3.1 Protein solutions

Hen egg white lysozyme (Sigma) was dissolved in 50 mM sodium acetate (Sigma-Aldrich) at pH 4.6 with 20% (w/v) glycerol (Fisher Scientific) at a concentration of ~100 mg/mL. Lysozyme concentrations were determined by UV absorbance measurements (Lambda 650 UV-Vis spectrophotometer, Perkin Elmer) at 280 nm using an extinction coefficient of 2.64 mL/(mg-cm).[20] For proof-of-concept crystallography experiments precipitant solutions of 1M and 2M NaCl (Aldrich) in 50 mM sodium acetate, pH 4.6 with 20% (w/v) glycerol were prepared. For screening experiments Crystal Screen chemicals were used directly (Hampton Research).

Thaumatin from *Thaumatococcus daniellii* (Sigma) was dissolved in 100 mM NaH_2PO_4 (EMD Chemicals) at pH 6.5 at a concentration of 82 mg/mL. The protein concentration was determined by UV absorbance measurements at 280 nm using an extinction coefficient of 1.25 mL/(mg-cm).[21] A precipitant solution of 30% (w/v) Na/K tartrate (Malinckrodt) and 20% w/v glycerol in 100 mM NaH_2PO_4 pH 7.0 was used.[22]

Ribonculease A (R-5500, Sigma) from bovine pancreas was dissolved in 100 mM sodium acetate at pH 4.5 at a concentration of 229 mg/mL. The protein concentration was determined by UV absorbance measurements at 280 nm using an extinction coefficient of 0.70 mL/(mg-cm).[23] A precipitant solution of saturated NaCl in 100 mM sodium acetate at pH 4.5 was used.[24]

Crystallization trials of the novel bacterial lyase were set up using 25 mg/mL concentration protein with 0.2 M ammonium acetate, 0.1 M HEPES and 25% PEG 3350 at pH 7.5.

Copper ATPase from *Thermus Thermophilus* was dissolved in 25 mM Tris at pH 7.5 along with 50 mM NaCl, 2 mM βME and 0.05% DMM. The protein concentration was determined to be 10 mg/mL and trials were set up using 0.1 M ammonium sulfate, 0.1 M HEPES Na at pH 7.5 and 18% v/v PEG 400 (condition 33 of the Memfac screen from Hampton Research)

Prior to setting up a crystallization experiment, protein solutions were filtered through 0.1 µm (Ultrafree-MC, Millipore) filters. Precipitant solutions were filtered through 0.22 µm (Steriflip, Millipore) filters.

2.3.2 Traditional crystallization experiments

Traditional microbatch-under-oil crystallization trials were set up combining 2 µL each of protein and precipitant solutions in a Greiner wellplate (Hampton Research) at room temperature. Paraffin oil was used to fill the microbatch tray before the trials were set up. Crystals from the microbatch experiments were harvested using Mitegen crystal mounts. Proof-of-concept crystallization trials of lysozyme in traditional wellplates as well as simple large well devices, and array chips were incubated at 4°C. Crystallization trials for thaumatin, ribonuclease A and Cu-ATPase were performed at room temperature. Crystallization trials for the novel bacterial lyase were set up at 9°C.

Crystallization trials and microfluidic chips were set up and visualized using either a stereomicroscope (Leica, MZ12.5) with an attached digital camera (Leica, DFC295) operated using Leica Application Suite software or a computer controlled imaging system comprised of an optical microscope (Leica Z16 APO) equipped with an auto-zoom lens (Leica 10447176), a digital camera (Leica DFC280), and a motorized x-y stage (Semprex KL66) controlled by Image Pro Plus (Media Cybernetics). For visualization of protein crystals, images were occasionally taken with the use of a cross-polarizer.

2.3.3 X-ray data collection and analysis

A majority of experiments were carried out at the 21-ID-F and 21-ID-G beamlines at the Advanced Photon Source at Argonne National Laboratory with the assistance of the Life Sciences Collaborative Access Team (LS-CAT). Samples were mounted on a standard magnetic goniometer mount (Hampton Research) with an attached metal tube into which a slit was cut and set-screw was used for securing samples. Data collection was performed either at room temperature or under cryogenic conditions. Cryocooling of samples was achieved by direct immersion into liquid nitrogen. Various sample-to-detector distances were used based on the quality of the crystal present. Typical data collection was done using a 1° oscillation with a 1 s exposure at an X-ray energy of 12.7 keV (λ = 0.979 Å). For merging slices of data from multiple crystals, 10° of data (-5° to +5° from the normal) was collected from various crystals in the device and an optimal subset of the frames was subsequently merged to obtain a complete dataset. Bench-top diffraction experiments were performed at the George L. Clark X-ray Facility at the University of Illinois using a Bruker General Area Diffraction Detector System (GADDS) equipped with a four circle diffractometer and HiStar multiwire area detector. A rotating anode

generator (Bruker M18XHF22) operating at 40 kV and 60 mA was used with a graphite monochromator supplying a Cu Kα radiation beam (λ = 1.54 Å or 8.048 keV). The sample to detector distance is ~18 cm. Data collection was done in a coupled mode where 2ω = 2θ such that multiple frames could be collected over a wider range of 2θ. Typically two such frames were collected, spanning the range of 2θ from 0° to 40° (up to 2.3 Å resolution).

Analysis of X-ray diffraction data collected at the synchrotron was performed using HKL2000 software for indexing, refinement, integration, and scaling (HKL Research Inc.).[25] Diffraction data collected at the University of Illinois was analyzed using the GADDS software (version 4.1.08, Bruker AXS) and Topas 3 (Bruker AXS). Subsequent processing of crystallography datasets was done using the CCP4 suite of programs.[26] Electron density maps were displayed using COOT.[27] Molecular replacement[28] for lysozyme was done using PDB structure 193L as a model.[29]

2.4 Conclusion

Here we have described the material characterization of COC which is the main component of the X-ray compatible microfluidic chips that are being designed. COC has a very low contribution to the scattering of the X-ray signal and has low attenuation compared to traditional microfluidic materials like PDMS and glass. The fabrication procedure for making multilayer microfluidics has also been described in detail, which will be used for making various microfluidic platforms described in Chapter 3.

2.5 Figures and Tables

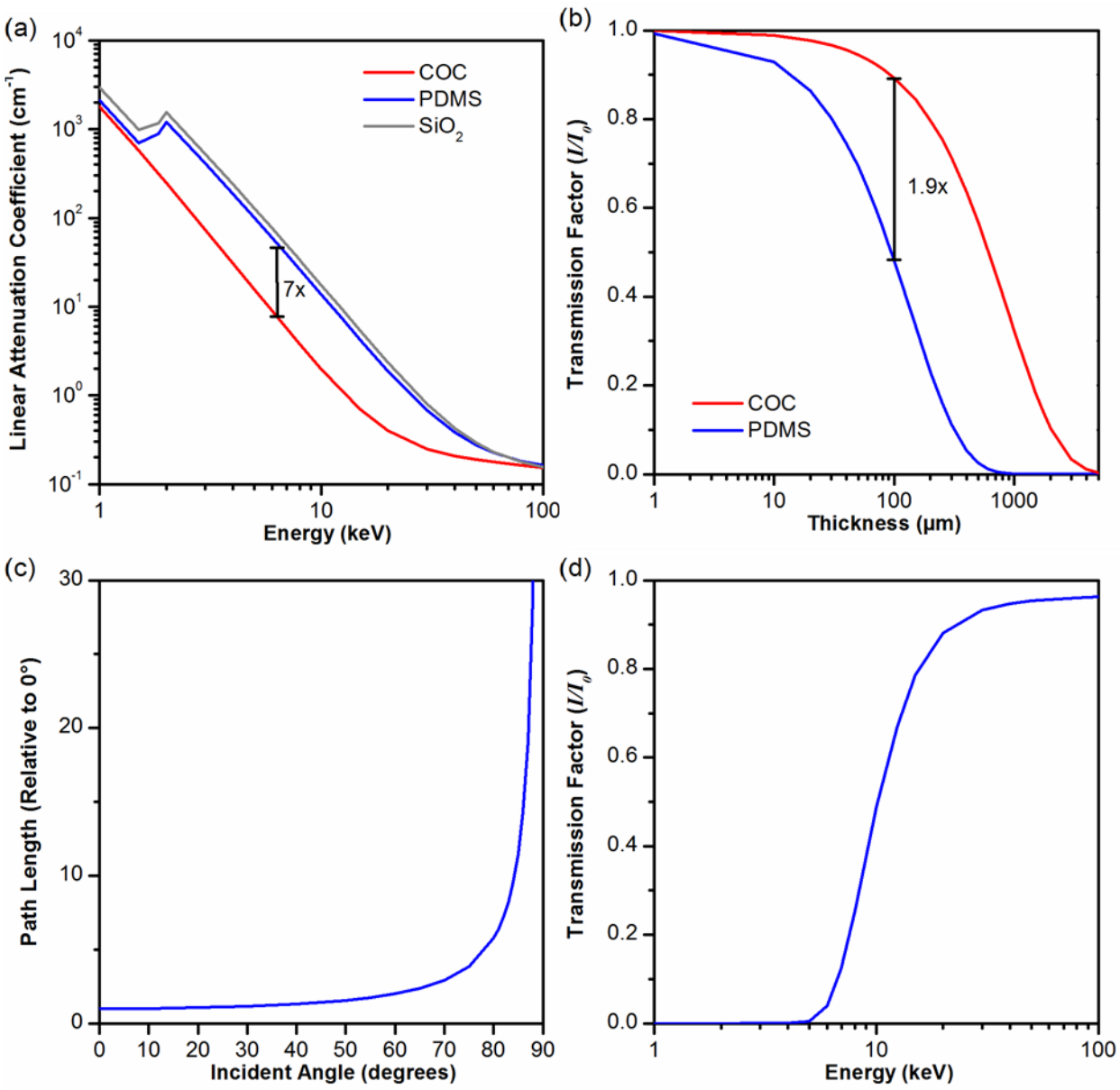

Figure 2.1: (a) Linear attenuation coefficient for PDMS, COC, and SiO_2 (quartz) as a function of photon energy. (b) Transmission factor I/I_0 as a function of film thickness for PDMS and COC. The transmission factor was calculated at a photon energy of 12.4 keV, or a wavelength of 1Å. (c) The relative path length through a material as a function of incident angle. Values for the path length have been normalized relative to the path length at 0° (normal incidence). (d) Transmission factor I/I_0 as a function of photon energy for a typical device architecture (50 μm COC substrate, 20 μm PDMS membrane, 175 μm COC control layer).

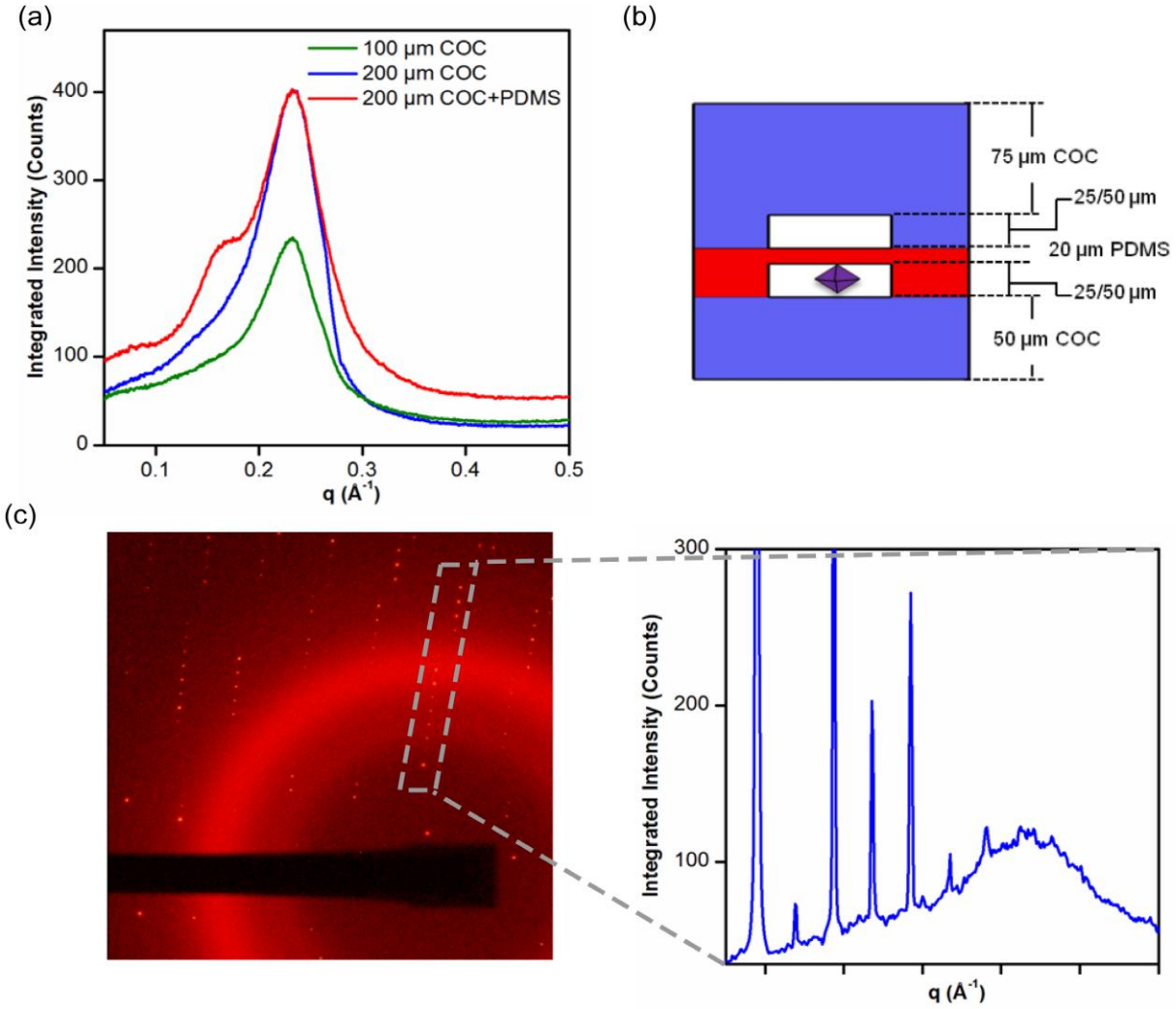

Figure 2.2: (a) Diffractograms showing the background scattering contribution of varying thicknesses of COC sheets (6013, Topas) with and without the presence of a thin PDMS membrane (< 30 µm). Scattering from COC occurs around $q \approx 0.232$ Å^{-1} (resolution of 5.2 Å). Scattering from PDMS occurs around $q \approx 0.161$ Å^{-1} (resolution of 7.5 Å). ($q = 4\pi\sin\theta/\lambda$ where 2θ is the scattering angle, λ is the X-ray wavelength). (b) Schematic depiction of the cross-section of a COC-PDMS device with the relative thicknesses of the various layers and the resultant crystals indicated. (c) Diffractogram of lysozyme grown in a COC-PDMS device showing both crystal diffraction and the background scattering contribution of the device. The diffraction signal resulting from the crystal is clearly visible above the diffuse scattering resulting from the device. A schematic depiction of the device and crystal with approximate thicknesses is given. The plot to the right is an area integration of the diffraction pattern highlighted in the image. (All data taken with the bench top source).

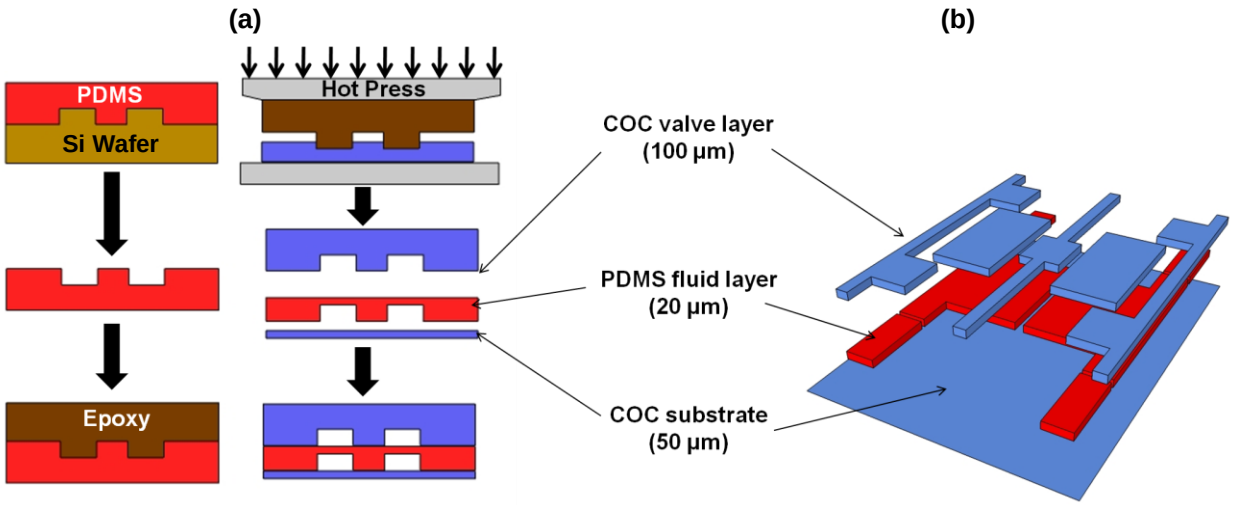

Figure 2.3: (a) Schematic showing the fabrication procedure for an X-ray transparent hybrid COC-PDMS-COC microfluidic chip. A PDMS replica is created from a patterned Si wafer, which is then used for replica molding a heat resistant epoxy master. The epoxy master is hot pressed with sheets of COC to transfer the pattern. The embossed COC control layer is bonded to a conventional PDMS fluid layer using chemical bonding and this assembly is bonded to a thin COC substrate. (b) 3-D exploded view of a well of an array mixing device showing the different layers

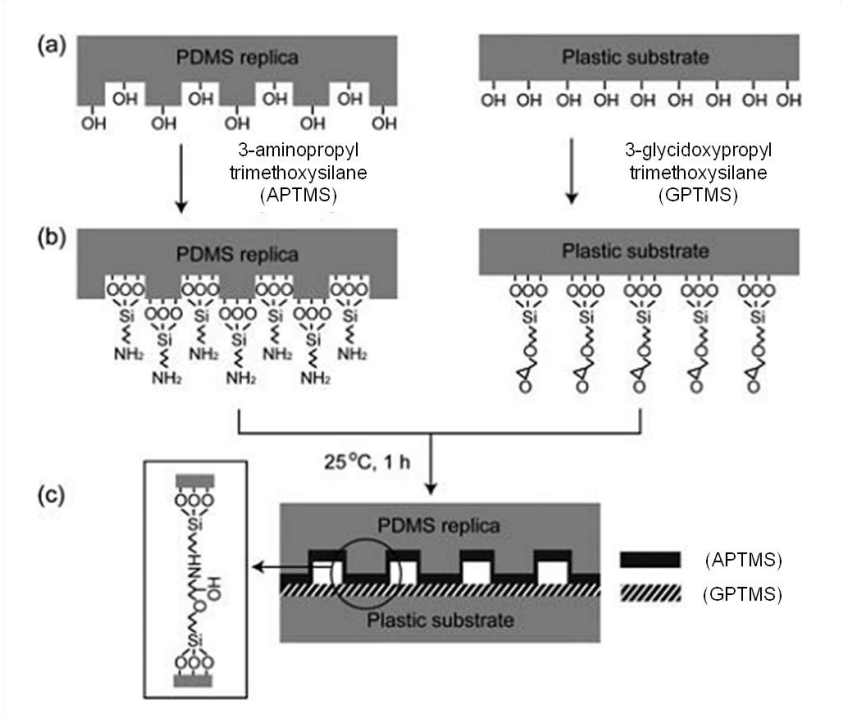

Figure 2.4: Surface hydroxylation of PDMS and plastic (COC) substrate by O_2 plasma treatment for 1 min. (b) Aminosilane and epoxysilane anchoring of the PDMS and COC plastic substrate. (c) Conformal contact of the two surfaces at room temperature for 1 hour. (Figure adapted from Tang and Lee, Lab Chip, 2010).[17]

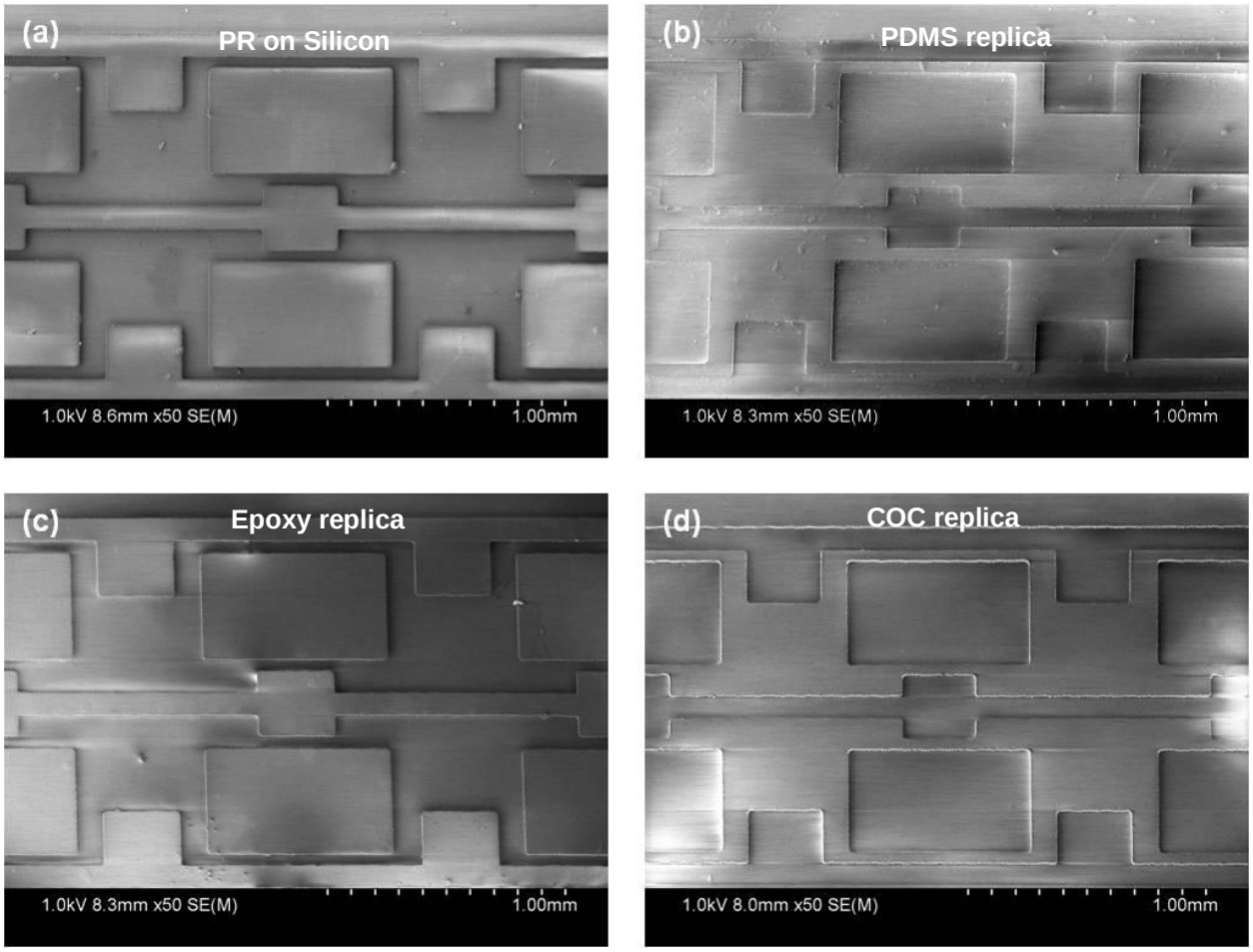

Figure 2.5: SEM images of a set of two wells in a 24 well array chip **(a)** silicon wafer patterned with SU-8-25, **(b)** the inverse PDMS mould created by replica moulding from the SU-8-25 on silicon pattern. **(c)** The epoxy master molded from the PDMS inverse master. **(d)** The final COC control layer fabricated via hot embossing using the epoxy master.

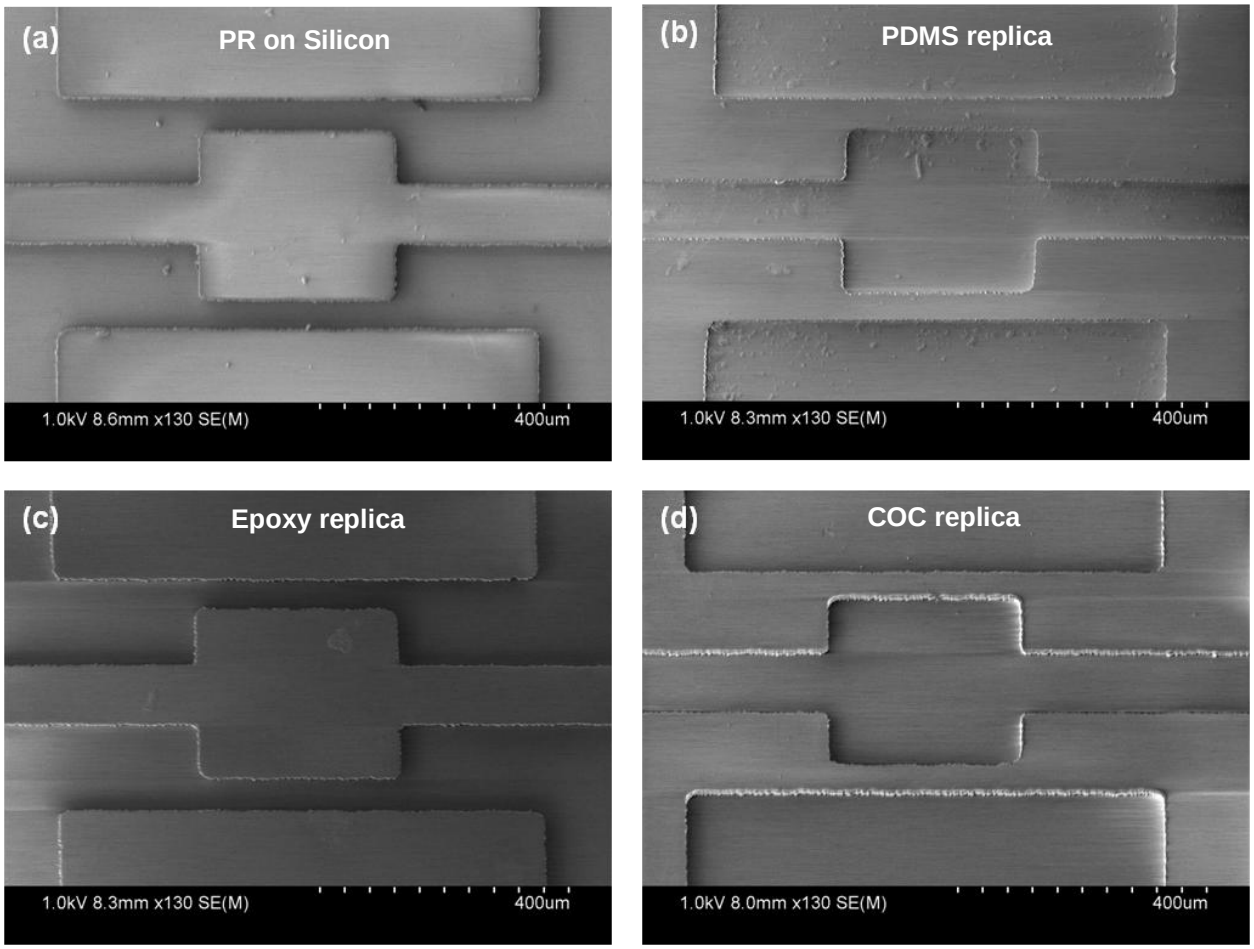

Figure 2.6: Close up SEM images of the middle mixing valve on a 24 well array chip **(a)** silicon wafer patterned with SU-8-25, **(b)** the inverse PDMS mould created by replica moulding from the SU-8-25 on silicon pattern. **(c)** The epoxy master molded from the PDMS inverse master. **(d)** The final COC control layer fabricated via hot embossing using the epoxy master.

Table 2.1: Atomic mass fraction, density, and a calculated value for the linear attenuation coefficient μ at 1Å (12.4 keV) for various materials used in microfluidic devices. SiO_2 = quartz[30], PDMS = polydimethylsiloxane ($Si_{61}O_{60}C_{124}H_{368}$), COC = cyclic olefin copolymer (C_9H_{14})[16], PMMA = polymethylmethacrylate (C_5H_8O)[16], PI = polyimide ($C_{22}H_{10}N_2O_5$).[30]

Element	SiO_2	PDMS	COC	PMMA	PI
H	--	0.08100	0.11546	0.09586	0.02636
C	--	0.32882	0.88454	0.71394	0.69118
N	--	--	--	--	0.07328
O	0.53257	0.21194	--	0.19020	0.20918
Si	0.46743	0.37824	--	--	--

Table 2.2: Oxygen permeability values (in cm^3–mm/m^2–day-atm) for materials commonly used in microfluidic devices.[11]

Material	Oxygen gas permeability (cm^3-mm/m^2-day-atm)	Water vapor transmission (g-mm/m^2-day)
PDMS	52531.0	125.0
PS	145.0	3.4-6
PU	78.7	0.9-3.43
COC	63.5	0.8
PETG	10.0	1.6
Parylene C	2.8	1.7

2.6 References

(1) Caffrey, M. *Ann Rev Biophys* **2009**, *38*, 29-51.
(2) Caffrey, M. *Cryst Growth Des* **2008**, *8*, 4244-4254.
(3) Cherezov, V.; Liu, J.; Griffith, M.; Hanson, M. A.; Stevens, R. C. *Cryst Growth Des* **2008**, *8*, 4307-4315.
(4) Liu, W.; Hanson, M. A.; Stevens, R. C.; Cherezov, V. *Biophys J* **2010**, *98*, 1539-1548.
(5) Sennoga, C.; Heron, A.; Seddon, J. M.; Templer, R. H.; Hankamer, B. *Acta Crystallogr D* **2003**, *59*, 239-246.
(6) Hubbell, J. H. S., S.M. *NIST Physical Reference Data* **1996**.
(7) Greaves, E. D.; Manz, A. *Lab Chip* **2005**, *5*, 382-391.
(8) Li, L.; Ismagilov, R. F. *Ann Rev Biophys* **2010**, *39*.
(9) Tsao, C.-W.; DeVoe, D. *Microfluid Nanofluid* **2009**, *6*, 1-16.
(10) Ro, K. W.; Liu, J.; Knapp, D. R. *Journal of Chromatography A* **2006**, *1111*, 40-47.
(11) Mehta, G.; Lee, J.; Cha, W.; Tung, Y. C.; Linderman, J. J.; Takayama, S. *Anal Chem* **2009**, *81*, 3714-3722.
(12) Piruska, A.; Nikcevic, I.; Lee, S. H.; Ahn, C.; Heineman, W. R.; Limbach, P. A.; Seliskar, C. J. *Lab Chip* **2005**, *5*, 1348-1354.
(13) Hansen, C. L.; Skordalakes, E.; Berger, J. M.; Quake, S. R. *P Natl Acad Sci USA* **2002**, *99*, 16531-16536.
(14) Unger, M. A.; Chou, H. P.; Thorsen, T.; Scherer, A.; Quake, S. R. *Science* **2000**, *288*, 113-116.
(15) Dhouib, K.; Malek, C. K.; Pfleging, W.; Gauthier-Manuel, B.; Duffait, R.; Thuillier, G.; Ferrigno, R.; Jacquamet, L.; Ohana, J.; Ferrer, J.-L.; Theobald-Dietrich, A.; Giege, R.; Lorber, B.; Sauter, C. *Lab Chip* **2009**, *9*, 1412-1421.
(16) Nunes, P.; Ohlsson, P.; Ordeig, O.; Kutter, J. *Microfluid Nanofluid*, *9*, 145-161.
(17) Tang, L.; Lee, N. Y. *Lab Chip* **2010**, *10*, 1274-1280.
(18) Schudel, B. R.; Choi, C. J.; Cunningham, B. T.; Kenis, P. J. A. *Lab Chip* **2009**, *9*, 1676-1680.
(19) Grover, W. H.; Skelley, A. M.; Liu, C. N.; Lagally, E. T.; Mathies, R. A. *Sensor Actuat B-Chem* **2003**, *89*, 315-323.
(20) Sophianopoulos, A. J.; Holcomb, D. N.; Vanholde, K. E.; Rhodes, C. K. *J Biol Chem* **1962**, *237*, 1107-1112.
(21) Charron, C.; Giege, R.; Lorber, B. *Acta Crystallogr D* **2004**, *60*, 83-89.
(22) Lopez-Jaramillo, F. J.; Garcia-Ruiz, J. M.; Gavira, J. A.; Otalora, F. *J Appl Crystallogr* **2001**, *34*, 365-370.
(23) Tessier, P. M.; Johnson, H. R.; Pazhianur, R.; Berger, B. W.; Prentice, J. L.; Bahnson, B. J.; Sandler, S. I.; Lenhoff, A. M. *Proteins* **2003**, *50*, 303-311.
(24) Talreja, S.; Perry, S. L.; Guha, S.; Bhamidi, V.; Zukoski, C. F.; Kenis, P. J. A. *The Journal of Physical Chemistry B* **2010**, *114*, 4432-4441.
(25) Otwinowski, Z.; Minor, W. *Macromolecular Crystallography, Pt A* **1997**, *276*, 307-326.
(26) *Acta Crystallogr D* **1994**, *50*, 760-763.

(27) Emsley, P.; Cowtan, K. *Acta Crystallographica Section D* **2004**, *60*, 2126-2132.
(28) Evans, P.; McCoy, A. *Acta Crystallographica Section D* **2008**, *64*, 1-10.
(29) Vaney, M. C.; Maignan, S.; Ries-Kautt, M.; Ducruix, A. *Acta Crystallographica Section D* **1996**, *52*, 505-517.
(30) *CRC Handbook of Chemistry and Physics*; 76th ed.; CRC Press: New York, **1996.**

Chapter 3

X-ray compatible microfluidic crystallization platforms for *in situ* protein crystallography

The design and operation of microfluidic platforms based on the materials and fabrication discussed previously have been presented in this chapter. First, a single well microfluidic chip is tested with various proteins to validate the device architecture for *in situ* data collection and analysis. Next, array chips have been utilized to screen for crystallization conditions of lysozyme. These array chips can also been used for *in situ* structure determination by merging slices of data from multiple crystals grown on-chip. A comparison of the relevant crystallographic statistics obtained from traditional and *in situ* microfluidic has also been presented.

3.1 Single well microfluidic chips for proof-of-concept studies

3.1.1 Design and operation

The single well chips for validating the X-ray compatibility of the materials consisted of a large rectangular well (2.36 mm by 3.36 mm) in the fluid layer, which was fabricated out of polydimethylsiloxane (PDMS). The height of the well was 25 µm with a total volume of 0.19 µL, and the total thickness of the fluid layer was 45 µm (schematic shown in Figure 3.1a). Six posts were fabricated within the fluidic well chamber to provide support for the thin PDMS membrane (20 µm thick). The control layer, fabricated out of cyclic olefin copolymer (COC), consisted of an identically sized chamber aligned directly above the well in the fluid layer (Figure 3.1a). Inlets for the fluid and the control layer were made with a 750 µm drill bit using a Dremel attached to a standard press setup. Then, oxygen plasma was used to bond the fluid and control layer. Since vacuum was used for the operation of this device, the fluid layer was reversibly bonded to the COC substrate.

After the protein crystals were grown in the well, the microfluidic device was mounted on a modified magnetic goniometer mount (Hampton Research) as shown in Figure 3.1b. A small, hollow, cylindrical metal tube with a narrow slit cut into the tube was glued onto the base of a standard goniometer mount. A set screw was fitted onto the top of this tube to ensure stability of the sample during data collection.

3.1.2 Validation of device architecture with single well microfluidic wells

The single well devices whose fabrication has been described above were used to validate the device architecture and test its efficacy for *in situ* protein crystallography. These wells were filled with premixed solutions of protein and precipitant for microbatch crystallization which under appropriate conditions led to protein crystals growing in the wells. The advantages of these simple well structures are that: (i) the overall device architecture could be tested independent of highly integrated chip designs and (ii) the wells are small enough to allow for cryogenic data collection. Crystals of soluble proteins lysozyme, ribonuclease A and thaumatin were grown on-chip (Figure 3.1c). Once the crystals were grown, the devices were trimmed down with a rotary cutter and mounted on a modified goniometer mount. Despite the device material surrounding the crystals, the samples could be cryocooled by plunging the mounted device into liquid nitrogen. However, the planar geometry of these devices were not suited for cryocooling, as the cryostream would occasionally shake the chip leading to difficulty in locating and centering the crystal for analysis. For simplicity, the crystals used in these experiments were grown in the presence of cryoprotectant, though in the future it should be possible to add cryoprotectant after crystals growth.

In situ data collection at the synchrotron from these samples under cryogenic conditions yielded good resolution data as can be seen in Figure 3.2. The individual X-ray diffraction spots are circular (insets in Figure 3.2) which indicate high crystal quality and low mosaicity. The expected scatter ring from the materials is present but did not hinder data analysis. To compare the quality of the data obtained *in situ* from a chip to that obtained using traditional methods, full cryogenic datasets for both a conventionally mounted lysozyme crystal grown using a traditional microbatch setup, and a crystal grown on-chip and analyzed *in situ* were obtained. A comparison of the important crystallographic parameters between the two crystals is presented in Table 3.1. Although the crystal mounted using traditional methods (which was bigger) diffracted to a better resolution, which could be accounted for by the nearly

order of magnitude difference in crystal size, other parameters like mosaicity, linear R-factor and completeness were comparable for both cases.

3.2 Microfluidic array chips for screening protein crystallization

The simple well microfluidic devices described in the previous section successfully validated the proposed device architecture for *in situ* X-ray crystallography. However, these devices do not take advantage of the advanced fluid handling capabilities offered by multilayer microfluidic networks. Microfluidic chips consisting of 24-wells were fabricated with automated fluid handling capabilities, which could not only be used for screening protein crystallization conditions, but could also be used subsequently for structure determination by merging datasets from multiple crystals grown in different wells.

3.2.1 Design and operation

The 24-well array chips consist of a dense network of actuate-to-open valves patterned over an array of wells (Figure 3.4a). These array chips consist of separate half-wells for protein and precipitant solutions, shown in the illustration in Figure 3.4a. The two half wells were filled independently of each other using dedicated valve lines for each set of half wells. Window structures were patterned in the control layer over each well to reduce the amount of material X-rays have to pass through thereby increasing the signal-to-noise ratio of the final diffraction pattern. The salient feature of this design is that it can be scaled up to even denser networks consisting of 96 wells, with the flexibility to vary the protein and precipitant ratios, and hence screen even more conditions. Figure 3.4b shows a schematic of a 96-well varied array chip where the protein and precipitant concentration are varied along the length of the chip.

Figure 3.5 describes the setup procedure of the array chips. Although the figure describes the process for a 24-well array chip, the procedure is similar for larger chips as well. First 2 µL of protein solution (more quantity will be needed for larger chips) was pipetted onto the protein line inlet and vacuum is applied through the corresponding valve line which allows dead filling of the protein into the series of half-wells (Figure 3.5b1-3). An improvement in the vacuum pressure within the chip can be achieved by sealing the various inlets with Scotch tape (3M) during filling. Once the protein has been filled the protein inlet and valve line were sealed with Crystal Clear tape (Hampton Resesarch). Next the

precipitant solution was loaded onto the chip by pipetting 1 µL droplets of precipitant solution onto each of the six precipitant inlet holes. Vacuum was then applied via the precipitant valve lines and the precipitant solutions filled into the appropriate half-wells (Figure 3.5c1-3). Next the mixing valves located between the protein and the precipitant half wells were actuated, allowing the two solutions to mix by free interface diffusion (Figure 3.5d1-3). Because mixing between the two half-wells occurs diffusively, these valves were maintained open for a period of time on the order of diffusive mixing time (~ 20 minutes). Depending upon the diffusivities of the various components in the crystallization trial, this mixing time can be optimized. After allowing the required time for mixing, the mixing valves were allowed to relax and the remaining inlets were sealed with Crystal Clear tape, following which the crystallization trials were allowed to incubate.

3.2.2 Screening of crystallization conditions

The 24-well microfluidic screening chips were designed for screening of various protein/precipitant combinations for batch crystallization. An individual chip allows for the testing of six different precipitant solutions in quadruplicate. A series of array chips was used to test each of the individual conditions in replicate wells and the results were compared to those obtained using a traditional microbatch wellplate. These microfluidic array chips were validated for crystallization screening experiments by testing solutions of ~100 mg/mL lysozyme in 50 mM sodium acetate pH 4.6 with 20% glycerol against the 50 condition Crystal Screen kit (Hampton Research) at room temperature.

After one week crystals were observed in 32 out of the 50 conditions in our array chips as compared to only 26 hits in the microbatch wellplate. Of the various hits observed between the traditional wellplate and our microfluidic chips, 21 of the conditions produced crystals on both platforms while five conditions yielded crystals uniquely in the microbatch wellplates and eleven hits were observed uniquely in the microfluidic devices. The variability between these results can be explained both in terms of differences in the mixing of protein and precipitant solutions, slow concentration of solutions in the microfluidic chips over time, and the stochastic nature and variability of the crystallization trials.[1] However, the performance of our microfluidic chips appears to be equal, if not better than that of traditional crystallization screening methods, and requires significantly smaller total volumes of protein.

Manual handling of crystals has the potential to impact the quality of diffraction from a crystal. Additionally, because of the difficulty in mounting crystals for analysis at room temperature the vast majority of crystals are only screened under cryogenic conditions, thus adding additional variables such as effects of the cryoprotectant and of the cryocooling process on the quality of the observed diffraction pattern. However, *in situ* analysis of crystal quality at room temperature using microfluidic devices was able to distinguish between protein and salt crystals, and was also able to provide information on the quality of the initial crystal hits. In addition to screening of crystal quality, complete or nearly complete room temperature datasets were collected for crystals grown in each of these conditions. Such information would have been significantly more difficult to obtain without *in situ* analysis capabilities. Table 3.2 provides a summary of the crystallographic statistics resulting from the analysis of a selection of the crystals and Table 3.4 lists these crystal forming conditions obtained from the crystallization screen.

3.3 Microfluidic chips for *in situ* structure determination from multiple crystals

For the purposes of dataset collection the array chips described earlier are too large, as currently designed, to be compatible with the cryostreams present on most beamlines. However, an alternative strategy is to collect small sections of data from multiple crystals which can then be merged together to obtain a full dataset. This method has been previously used for obtaining structural information from tiny or fragile crystals or crystals which suffer from excessive radiation damage[2,3] and is relatively common in time resolved and Laue crystallography.[4-6] The array chips described earlier can be used for this method of data collection by filling in the same precipitant condition in all the precipitant wells. Thus, a large number of crystals can be grown on-chip which can be then analyzed *in situ*. The fine control over fluid transport on the microfluidic scale should also help to improve the potential for reproducibility of crystal quality between different wells. To demonstrate this method, lysozyme crystals were grown in a 24-well array chip using the same crystallization conditions as the simple well and traditional microbatch crystallization trials. An optical micrograph of the chip is shown in Figure 3.6a.

For each of the crystals grown on this chip 10° of X-ray data was collected (-5° to +5° from normal). These datasets were then integrated individually using HKL2000, and then were scaled together using the scaling function in HKL2000. Different crystallographic parameters were obtained from the log file post-analysis. A comparison of the various crystallographic parameters obtained using this method,

the cryogenic data collected from a single crystal on-chip and the data collected from a single crystal mounted using traditional methods (Table 3.3) shows the quality of the data to be unaffected by collection at room temperature or because of the use of multiple crystals. In terms of the resolution and completeness, the merged data compares well with the data collected from a single crystal. For an even comparison, the data from the single crystals were reanalyzed to the same resolution obtained from merging. This allowed for a better comparison for the other statistics as refining the resolution to a lower value has an effect on all the parameters. The area where the room temperature data excelled compared to either cryogenic dataset is crystal mosaicity, despite the potential for increased radiation damage in room temperature data collection. The lack of physical handling and cryocooling of the crystals grown in the array chip, resulted in the mosaicity for the merged data being an order of magnitude lower than that collected from the single crystals under cryogenic conditions. The observed mosaic spread of the crystals was nearly an order of magnitude smaller than that of the cryogenic samples. Additionally, this small range of mosaicity was consistent for nearly all of the crystals grown in the 24-well chip. This consistency validates the reproducibility of well-to-well crystallization, in particular demonstrating fine control of fluid transport and thus crystallization kinetics.

The I/σ ratio describes the signal-to-noise ratio of the observed diffraction spots. A comparison of I/σ in the various crystals analyzed allows for determination of the impact of signal attenuation and background scatter from device materials as compared to traditional cryogenic crystal mounting methods. For the data collected from the three different methods at equivalent resolution, the overall I/σ ratio is best for the merged data, but for the data in the highest resolution shell (shown in parenthesis in Table 3.3) the merged data has the lowest I/σ ratio. This would explain why the merged data is the limiting factor in terms of resolution, because the better the data is in the higher resolution shells, higher resolution data is obtained.

The next statistic of importance is the R_{free} or R-factor. These R-factors are an indication of how well the refined structure agrees with the observed electron density maps. Electron density maps for the three different data collection methods are shown in Figure 3.7. The free R-factor (R_{free}) provides a metric for cross-validating the quality of the structural model by comparing it with a small test set of "free" reflections which were not used in the refinement of the model.[7,8] In general, for a structure determination

made with data to 2.0 Å resolution, the final R-factor would be expected to be ~20%, with R_{free} a few percent higher.[8] As can be seen from the data presented in Table 3.3, for all of the data collection strategies, the data extended beyond 2.0 Å and resulted in R-factors < 20%. Another interesting observation is that the R-factor for data collected on-chip is lower than those obtained for traditional methods.

3.4 Conclusion

Here we have used lysozyme, a robust model protein to validate our microfluidic chips for *in situ* analysis. While the results described above prove that the microfluidic chips are suitable for *in situ* structure determination, a need to solve structures of novel proteins to establish this as a general method for structure determination is still required. Crystals of bacterial defluorinase (Figure 3.8a) and a novel bacterial lyase (Figure 3.8b) have been successfully crystallized on-chip. Work is presently on in optimizing the crystallization condition to grow more robust crystals in order to get high resolution data of these novel proteins.

3.5 Figures and tables

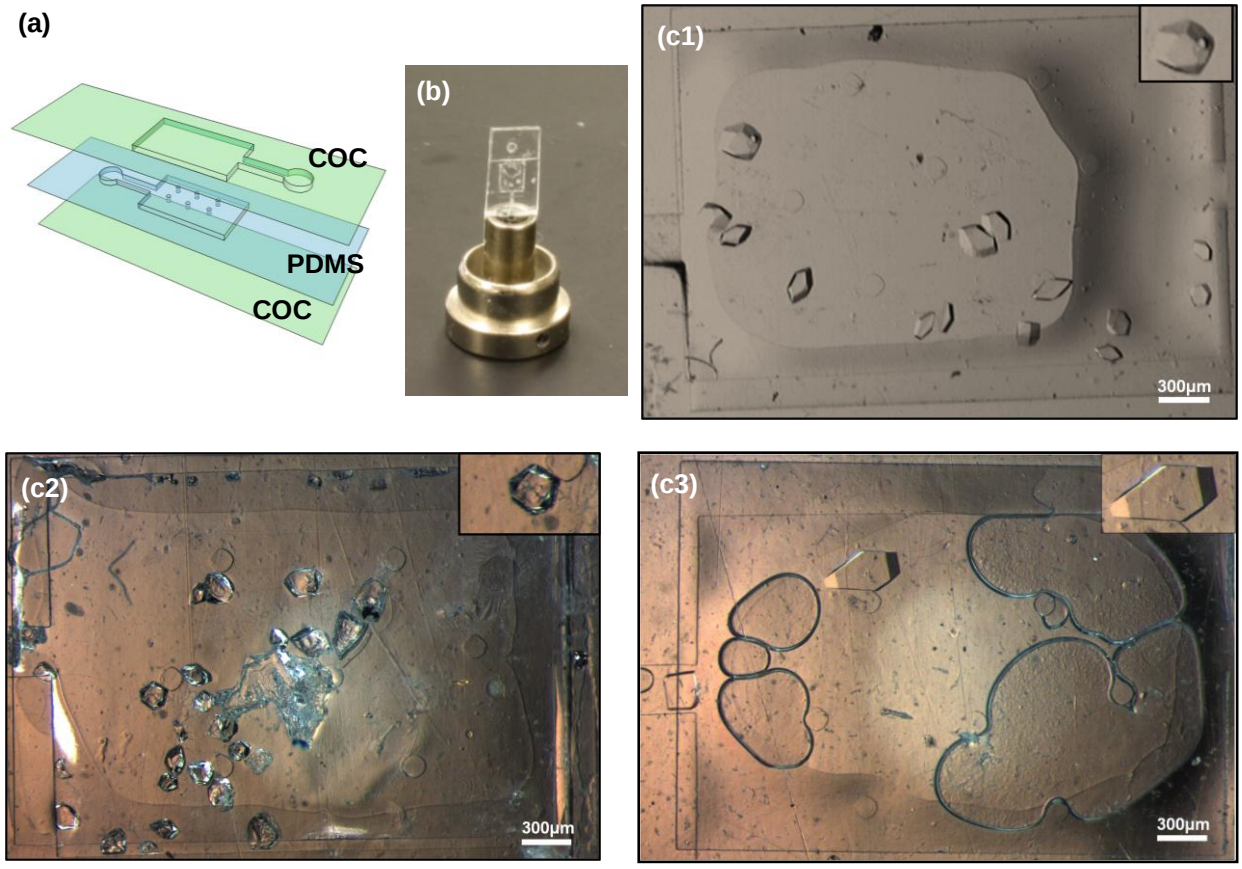

Figure 3.1: (a) Schematic depiction of a single well device. A large rectangular well with support posts is molded in PDMS (blue) and aligned with a matching COC control layer and substrate (green). The entire assembly is then attached to a COC substrate. (b) A large well device mounted on a modified magnetic goniometer mount. Optical micrographs of (c1) lysozyme, (c2) thaumatin, and (c3) ribonuclease A crystals grown on-chip.

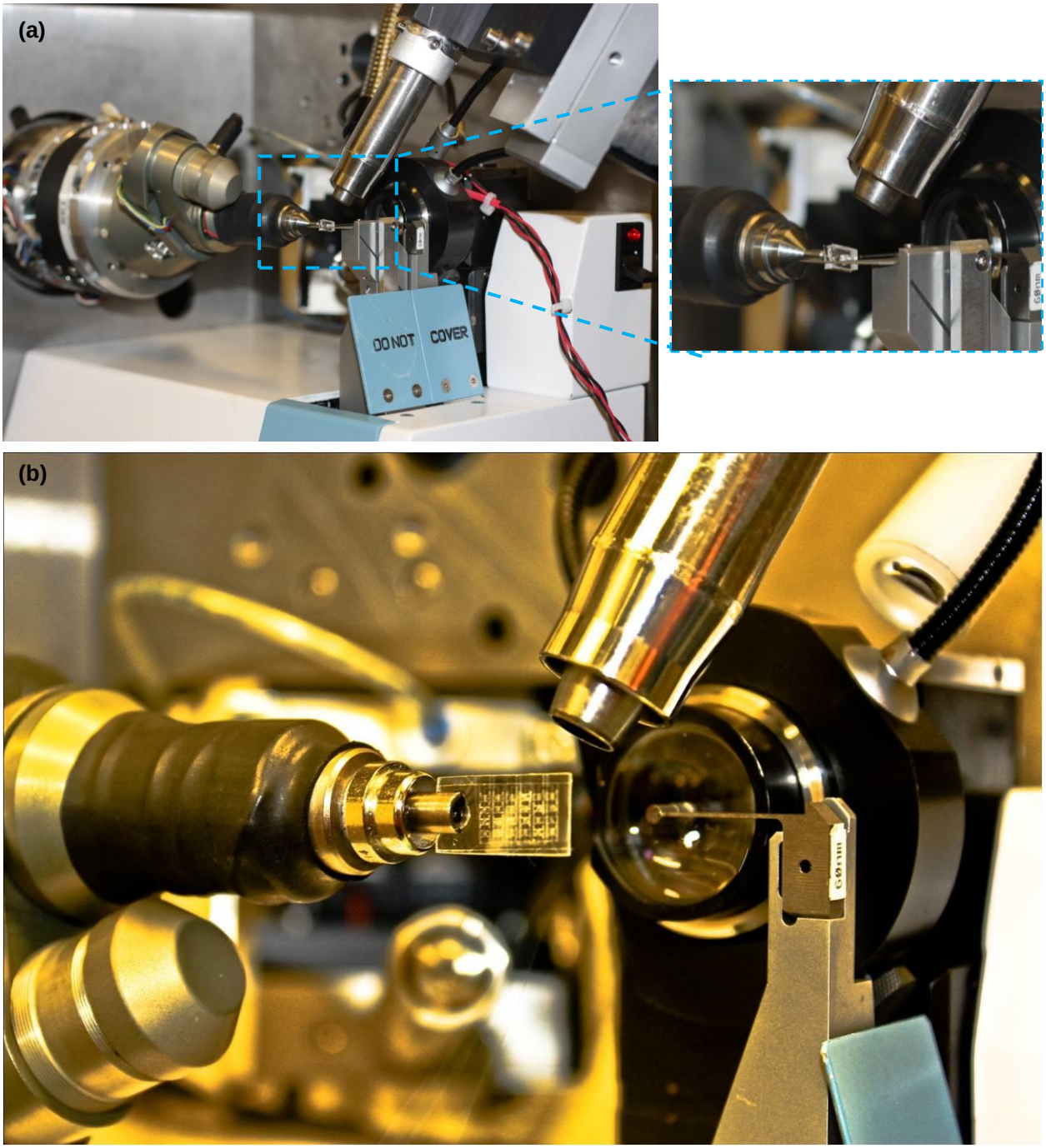

Figure 3.2: Photograph of (a) a single well microfluidic chip and (b) a 24-well array chip mounted on beamline 21ID-G at LSCAT, Advanced Photon Source, Argonne National Lab.

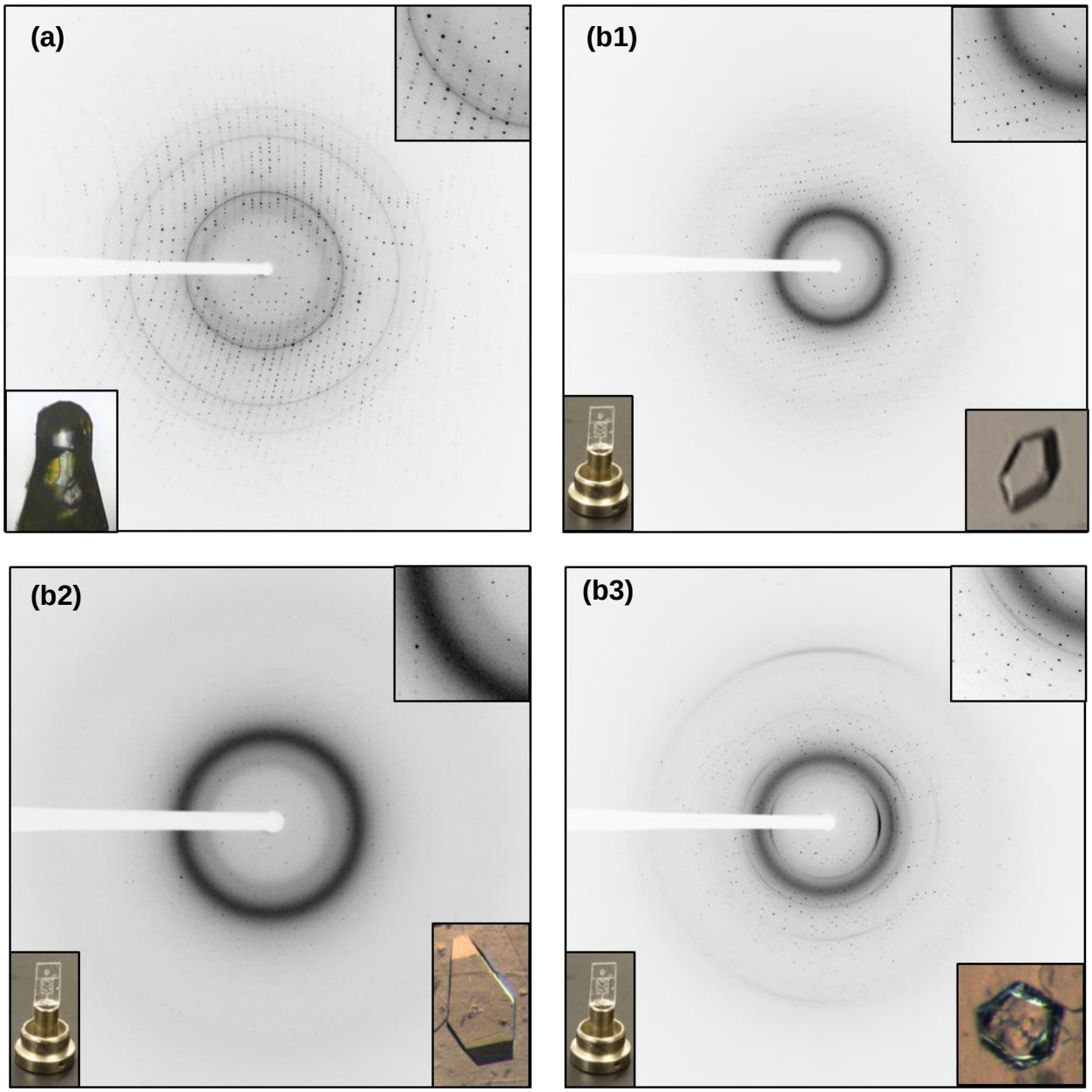

Figure 3.3: X-ray diffraction data collected under cryogenic conditions at LS-CAT, APS. (a) Data from a lysozyme crystal grown using the traditional microbatch method and mounted on a standard crystal mount. (b) Data from (b1) lysozyme (b2) thaumatin and (b3) ribonuclease A crystals grown in a large well hybrid COC-PDMS chip and analyzed *in situ*. Insets on the upper-right provide a closer view of spot quality. On the lower-right optical micrographs are shown of crystals growing within their respective trays or chips. The inset on the lower-left is a photograph of the mounted crystal, either in a mount or in a chip. Lysozyme data were collected using a sample-to-detector distance of 100 mm while Thaumatin and ribonuclease A data were taken at a distance of 150 mm.

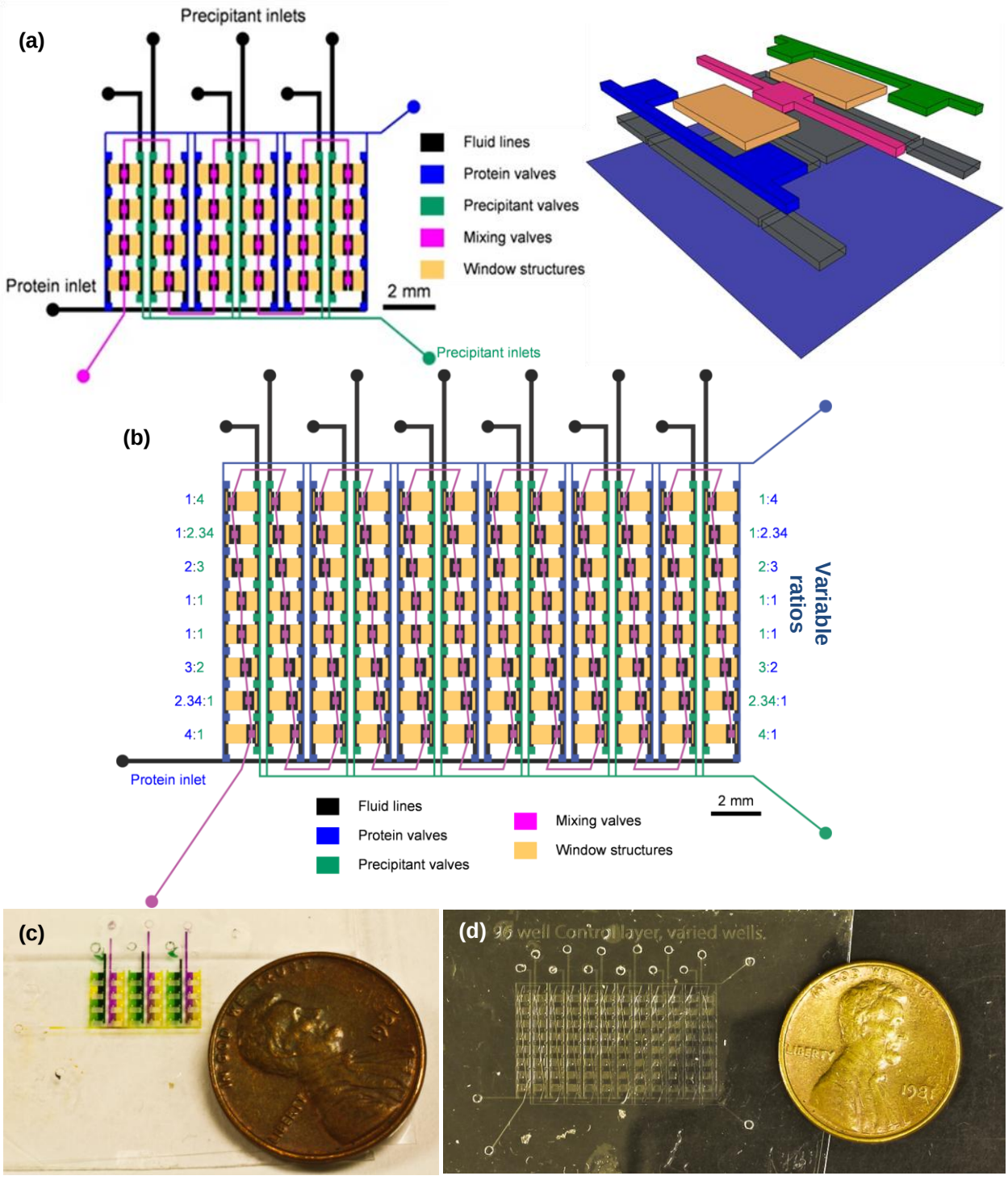

Figure 3.4: (a) Schematic of the 24-well array chip showing the various valve lines and the fluid lines for filling in the protein and precipitant. The valves and fluid lines are color coordinated with the 3-dimensional exploded view shown to the right. The fluid lines are shown in black, valves to fill in protein chambers are in blue, and valves to fill in precipitant chambers are shown in green. The pink mixing valves are used to connect the two chambers and mix the protein and precipitant by free interface diffusion. The yellow window structures serve the purpose of decreasing the amount of material in the X-ray beam path. (b) Schematic of a 96-well array chip with variable protein to precipitant ratio for screening crystallization conditions of proteins. The color coding is the same as above. (c) Optical micrograph of food coloring filled in a 24-well array chip. (d) Optical micrograph of a 96-well varied well array chip.

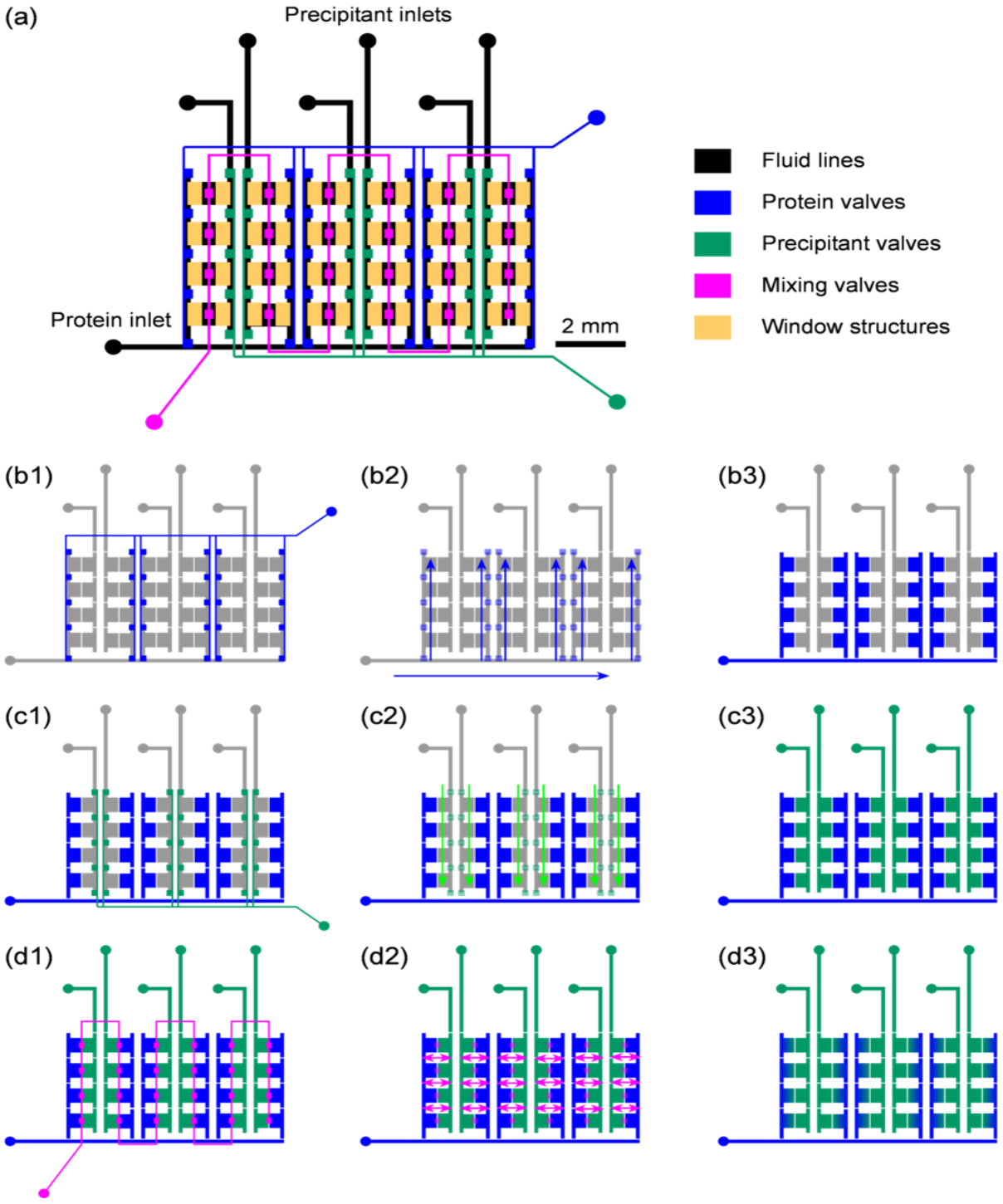

Figure 3.5: Schematic depiction of the design and operation of a 24-well microfluidic array chip for the crystallization of soluble or detergent solubilized proteins. (a) The complete device. Protein and precipitant inlets are indicated. The fluid layer is shown in black while the various features of the control layer have been identified based on function. Valves for the loading of protein are shown in blue, precipitant valves in green, and the valves to connect chambers and allow for diffusion between the protein and precipitant chambers are pink. Yellow window structures are shown in yellow. These structures are present in the control layer, but serve only to decrease the thickness of material present in the path of the X-ray beam. (b-d) Depiction of device operation. (b) Blue valves are actuated to fill in protein solution. (c) Green valves actuate to fill in precipitant solutions. (c) Pink valves actuate to connect the protein and precipitant chambers, allowing for diffusion over time

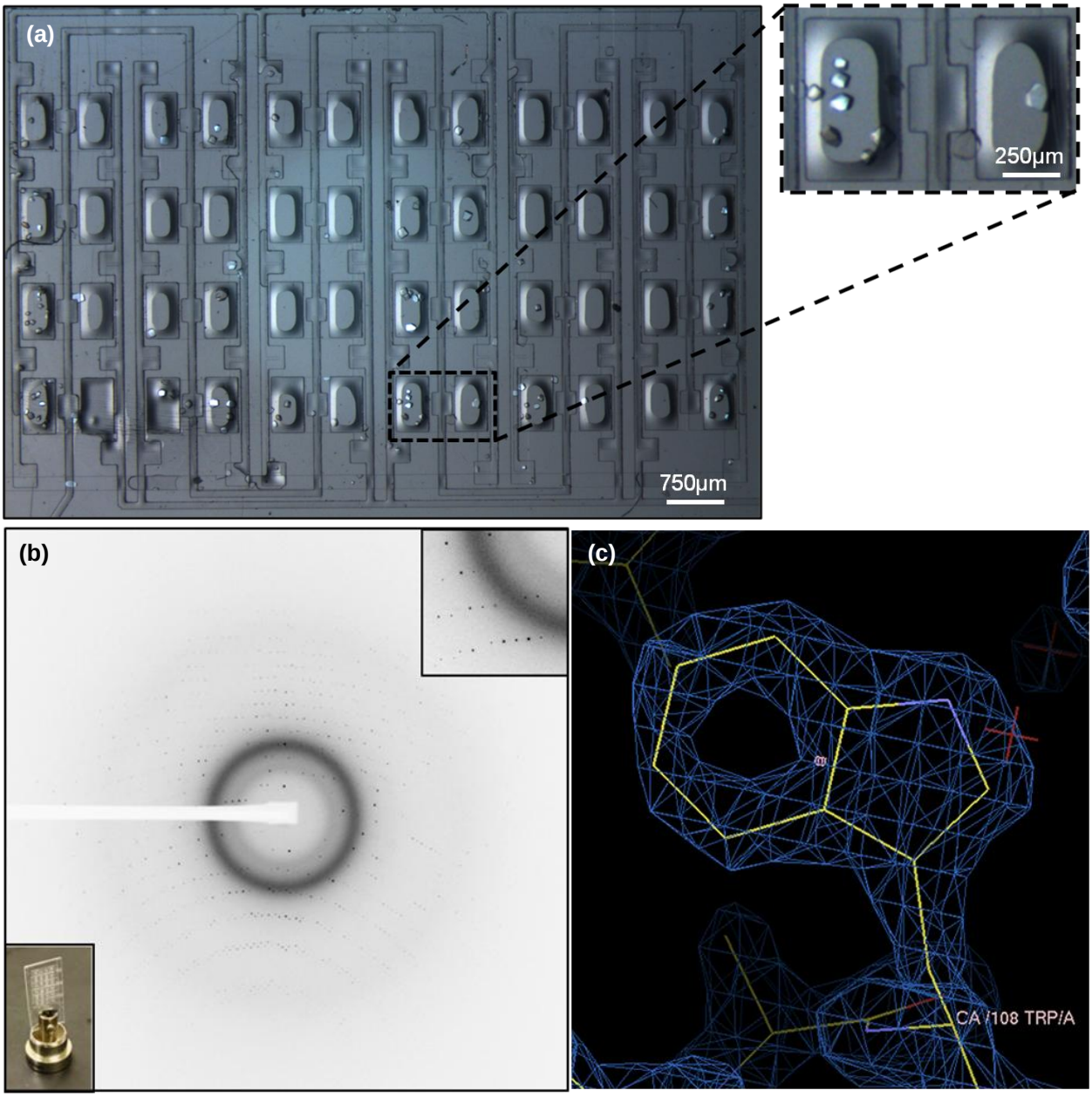

Figure 3.6: (a) Optical micrograph of a 24-well hybrid COC-PDMS device containing lysozyme crystals grown on-chip. Slices of data from these multiple crystals were merged to get a complete dataset. (b) Diffraction data from a lysozyme crystal grown in 24-well array device and analyzed *in situ* at room temperature. The inset on the upper-right provides a closer view of spot quality. On the lower-right an optical micrograph is shown of crystals growing in the chip. The inset on the lower-left is a photograph of the mounted chip. Sample to detector distance was 200 mm. (c) An electron density map (map display at σ = 2.1) of a single tryptophan residue (W108) after molecular replacement and a single round of model building. The conformation and electron density of the aromatic side chain is clearly visible.

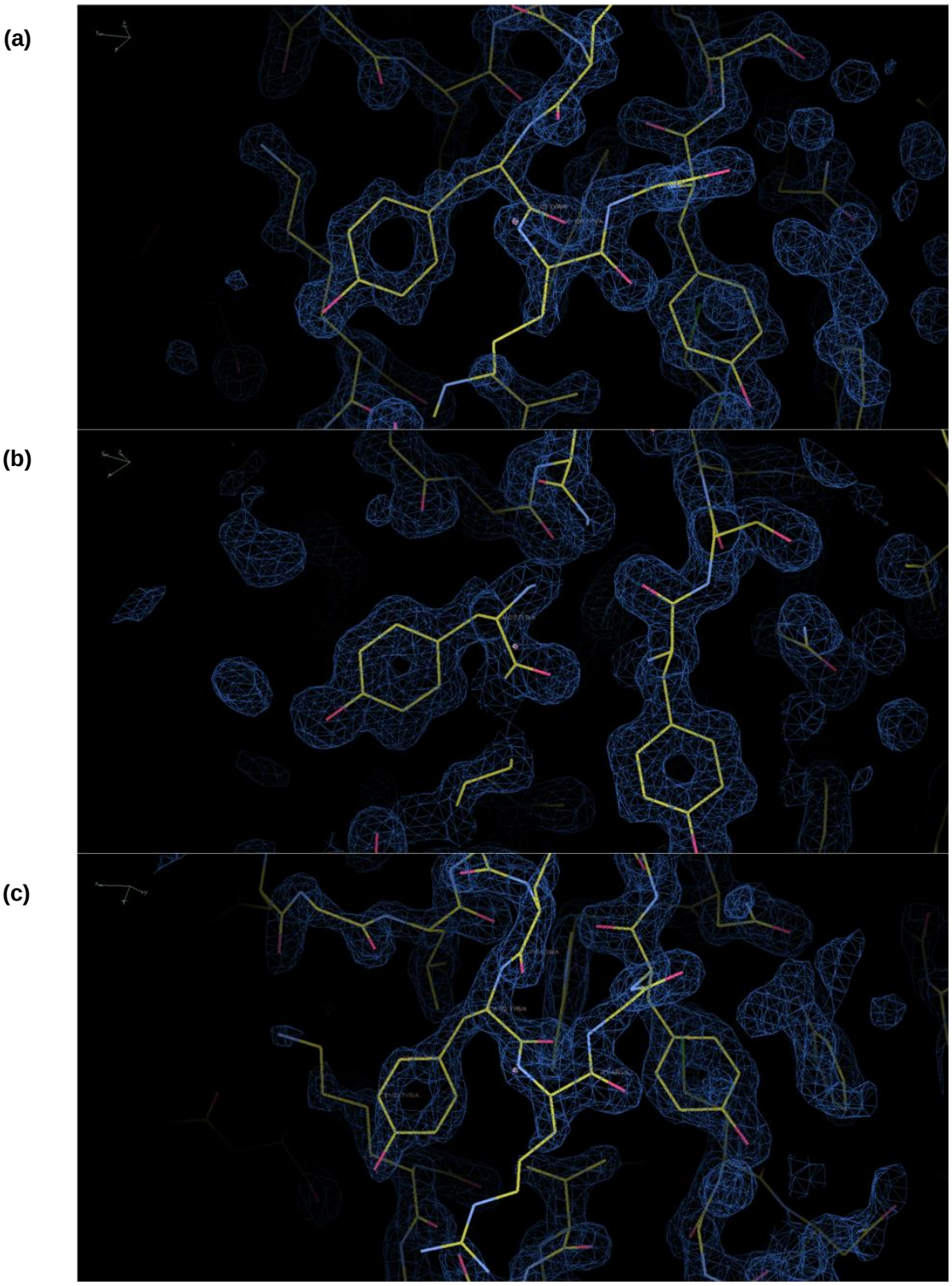

Figure 3.7: Electron density maps of lysozyme taken to 1.55Å (a) grown in a traditional microbatch wellplate an mounted using conventional methods and (b) grown on a large well microfluidic device. (c) Electron density map of data obtained by merging data from many lysozyme crystals grown on-chip. All three maps correspond to the structure of Tyrosin (Tyr) at a sigma level of 2.0.

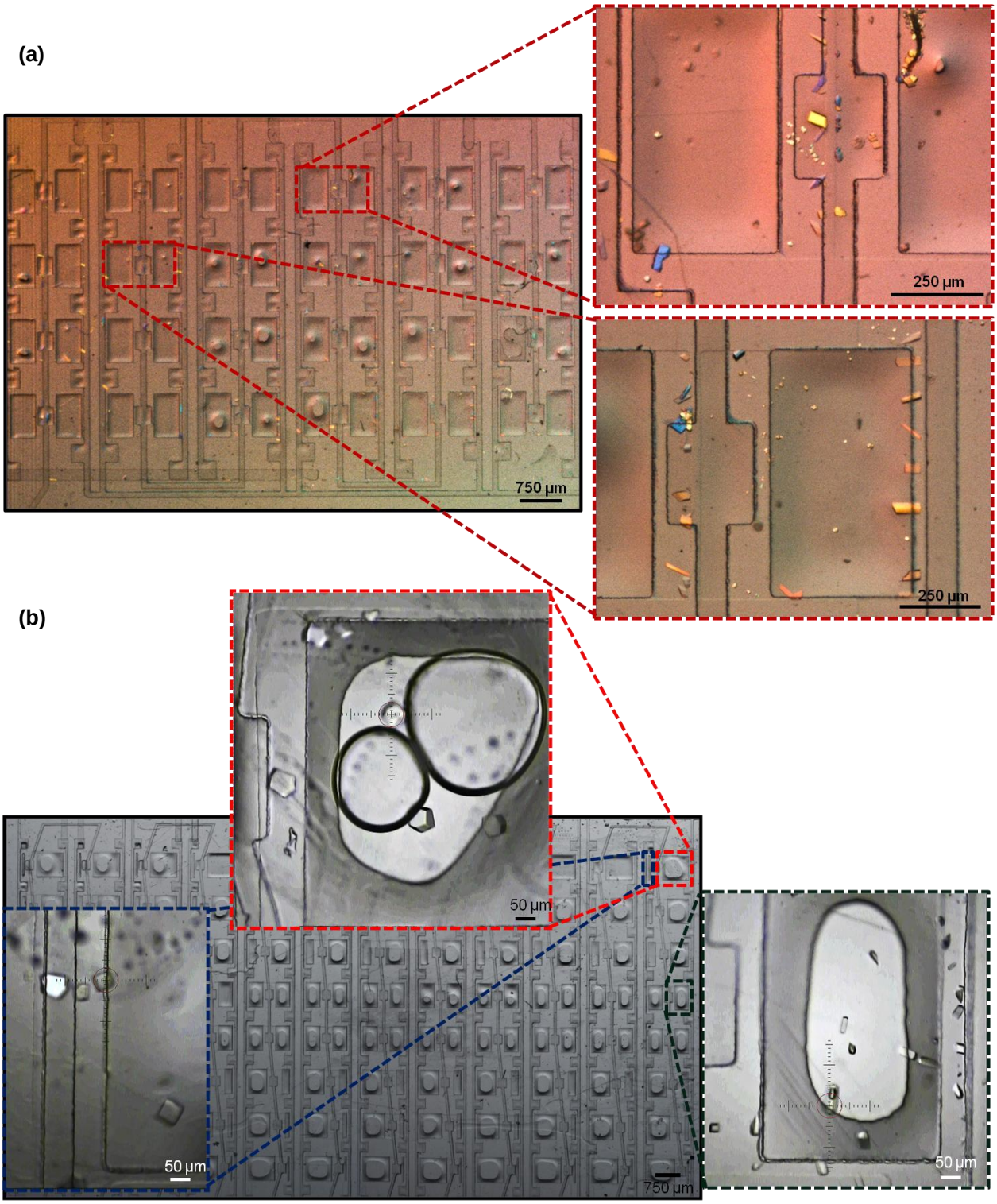

Figure 3.8: (a) Optical micrograph of a 24-well array device with crystals of bacterial defluorinase grown on-chip. (b) Optical micrograph of a varied 96-well array device with crystals of novel bacterial lyase grown on-chip. The different forms of crystals are clearly visible in the insets of chambers with different ratios of protein to precipitant.

Table 3.1: Crystallographic data statistics from the analysis of two lysozyme crystals under cryogenic conditions, the first one mounted using traditional methods and the other grown on-chip and analyzed *in situ*. Values in parenthesis are for the highest resolution shell.

Parameter	Traditional Cryogenic	Microfluidic Single Crystal
Resolution	50 - 1.25 Å	50 - 1.35 Å
R_{sym}	0.058 (0.338)	0.078 (0.488)
Mosaicity	0.21 - 0.33°	0.27 - 0.41°
Redundancy	7.4 (5.8)	7.6 (6)
Completeness	99.1% (98.5%)	95.9% (98.8%)
I/sigma	33.8 (3.7)	25.8 (3.4)
Frames	1 - 100	3-100

Table 3.2: Crystallographic data statistics from the analysis of lysozyme crystals crystallized via the Hampton screening kit, all the crystals were grown on-chip and were analyzed *in situ* at room temperature. Values in parenthesis are for the highest resolution shell.

Parameter	Crystal Screen Reagent			
	30	**33**	**34**	**40**
Resolution	50 - 1.75 Å	50 - 1.70 Å	50 - 1.60 Å	50 - 1.55 Å
Rsym	0.075 (0.300)	0.050 (0.365)	0.044 (0.302)	0.041 (0.281)
Mosaicity	0.08 - 0.27°	0.20 - 0.50°	0.15 - 0.20°	0.04 - 0.18°
Redundancy	4.3 (2.7)	6.2 (5.3)	5.3 (4.4)	5.7 (3.5)
Completeness	91.9% (77.3%)	97.5% (96.5%)	97.3% (93.4%)	99.4% (95.2%)
I/sigma	21.2 (3.2)	37.0 (4.0)	34.7 (4.5)	32.7 (4.2)

Table 3.3: Comparison of crystallographic data statistics from the analysis of lysozyme crystals crystallized via (a) "traditional" microbatch method and mounted using a standard crystal mount (b) cryogenic analysis of a "single crystal" grown in a large well device and (c) merging of datasets from "multiple crystals" grown in a 24-well array chip. Values in parenthesis are for the highest resolution shell. The data for the cryogenic samples have been reanalyzed over the resolution range of 50-1.55 Å to enable direct comparison with merged data.

Parameter	Traditional Cryogenic		Microfluidic Single Crystal		Microfluidic Multi-Crystal Room Temperature
	Complete	**Matched to merged data**	**Complete**	**Matched to merged data**	
Resolution	50 - 1.25 Å	50 - 1.55 Å	50 - 1.35 Å	50-1.55 Å	50 - 1.55 Å
R_{sym}	0.058 (0.338)	0.052 (0.102)	0.078 (0.488)	0.072(0.217)	0.064 (0.362)
Mosaicity	0.21 - 0.33°	0.21 - 0.34°	0.27 - 0.41°	0.27-0.45	0.03-0.08
Redundancy	7.4 (5.8)	7.7 (7.7)	7.6 (6)	7.9(7.8)	22.9 (5.7)
Completeness	99.1% (98.5%)	99.7% (100%)	95.9% (98.8%)	94.7% (98.1%)	98.1% (83.4%)
I/sigma	33.8 (3.7)	42.3 (19.4)	25.8 (3.4)	30.3 (10)	51.4 (3.9)
Frames	100	100	98	98	363
	Refinement				
R (R_{free})		0.173 (0.276)		0.162 (0.212)	0.164 (0.227)

Table 3.4: Summary of the crystallization results of a microfluidic batch screen of 96 mg/mL lysozyme in 50 mM sodium acetate pH 4.6 with 20% glycerol against the 50 condition Hampton Crystal Screen at room temperature.

Reagent #	Crystallization Solution
6	0.2 M Magnesium chloride hexahydrate, 0.1 M TRIS hydrochloride pH 8.5, 30% w/v Polyethylene glycol 4,000
7	0.1 M Sodium cacodylate trihydrate pH 6.5, 1.4 M Sodium acetate trihydrate
8	0.2 M Sodium citrate tribasic dihydrate, 0.1 M Sodium cacodylate trihydrate pH 6.5, 30% v/v 2-Propanol
9	0.2 M Ammonium acetate, 0.1 M Sodium citrate tribasic dihydrate pH 5.6, 30% w/v Polyethylene glycol 4,000
10	0.2 M Ammonium acetate, 0.1 M Sodium acetate trihydrate pH 4.6, 30% w/v Polyethylene glycol 4,000
11	0.1 M Sodium citrate tribasic dihydrate pH 5.6, 1.0 M Ammonium phosphate monobasic
12	0.2 M Magnesium chloride hexahydrate, 0.1 M HEPES sodium pH 7.5, 30% v/v 2-Propanol
15	0.2 M Ammonium sulfate, 0.1 M Sodium cacodylate trihydrate pH 6.5, 30% w/v Polyethylene glycol 8,000
16	0.1 M HEPES sodium pH 7.5, 1.5 M Lithium sulfate monohydrate
17	0.2 M Lithium sulfate monohydrate, 0.1 M TRIS hydrochloride pH 8.5, 30% w/v Polyethylene glycol 4,000
18	0.2 M Magnesium acetate tetrahydrate, 0.1 M Sodium cacodylate trihydrate pH 6.5, 20% w/v Polyethylene glycol 8,000
19	0.2 M Ammonium acetate, 0.1 M TRIS hydrochloride pH 8.5, 30% v/v 2-Propanol
20	0.2 M Ammonium sulfate, 0.1 M Sodium acetate trihydrate pH 4.6, 25% w/v Polyethylene glycol 4,000
21	0.2 M Magnesium acetate tetrahydrate, 0.1 M Sodium cacodylate trihydrate pH 6.5, 30% v/v (+/-)-2-Methyl-2,4-pentanediol
22	0.2 M Sodium acetate trihydrate, 0.1 M TRIS hydrochloride pH 8.5, 30% w/v Polyethylene glycol 4,000
23	0.2 M Magnesium chloride hexahydrate, 0.1 M HEPES sodium pH 7.5, 30% v/v Polyethylene glycol 400
25	0.1 M Imidazole pH 6.5, 1.0 M Sodium acetate trihydrate
27	0.2 M Sodium citrate tribasic dihydrate, 0.1 M HEPES sodium pH 7.5, 20% v/v 2-Propanol
28	0.2 M Sodium acetate trihydrate, 0.1 M Sodium cacodylate trihydrate pH 6.5, 30% w/v Polyethylene glycol 8,000
29	0.1 M HEPES sodium pH 7.5, 0.8 M Potassium sodium tartrate tetrahydrate
30	0.2 M Ammonium sulfate, 30% w/v Polyethylene glycol 8,000
31	0.2 M Ammonium sulfate, 30% w/v Polyethylene glycol 4,000
32	2.0 M Ammonium sulfate
33	4.0 M Sodium formate
34	0.1 M Sodium acetate trihydrate pH 4.6, 2.0 M Sodium formate
35	0.1 M HEPES sodium pH 7.5, 0.8 M Sodium phosphate monobasic monohydrate, 0.8 M Potassium phosphate monobasic
36	0.1 M TRIS hydrochloride pH 8.5, 8% w/v Polyethylene glycol 8,000
37	0.1 M Sodium acetate trihydrate pH 4.6, 8% w/v Polyethylene glycol 4,000
38	0.1 M HEPES sodium pH 7.5, 1.4 M Sodium citrate tribasic dihydrate
39	0.1 M HEPES sodium pH 7.5, 2% v/v Polyethylene glycol 400, 2.0 M Ammonium sulfate
40	0.1 M Sodium citrate tribasic dihydrate pH 5.6, 20% v/v 2-Propanol, 20% w/v Polyethylene glycol 4,000
41	0.1 M HEPES sodium pH 7.5, 10% v/v 2-Propanol, 20% w/v Polyethylene glycol 4,000
42	0.05 M Potassium phosphate monobasic, 20% w/v Polyethylene glycol 8,000
43	30% w/v Polyethylene glycol 1,500
44	0.2 M Magnesium formate dihydrate
45	0.2 M Zinc acetate dihydrate, 0.1 M Sodium cacodylate trihydrate pH 6.5, 18% w/v Polyethylene glycol 8,000
46	0.2 M Calcium acetate hydrate, 0.1 M Sodium cacodylate trihydrate pH 6.5 , 18% w/v Polyethylene glycol 8,000
47	0.1 M Sodium acetate trihydrate pH 4.6, 2.0 M Ammonium sulfate
48	0.1 M TRIS hydrochloride pH 8.5, 2.0 M Ammonium phosphate monobasic

3.6 References

(1) Newman, J.; Xu, J.; Willis, M. C. *Acta Crystallographica Section D* **2007**, *63*, 826-832.
(2) Jaakola, V. P.; Griffith, M. T.; Hanson, M. A.; Cherezov, V.; Chien, E. Y. T.; Lane, J. R.; IJzerman, A. P.; Stevens, R. C. *Science* **2008**, *322*, 1211-1217.
(3) Cherezov, V.; Rosenbaum, D. M.; Hanson, M. A.; Rasmussen, S. G. F.; Thian, F. S.; Kobilka, T. S.; Choi, H. J.; Kuhn, P.; Weis, W. I.; Kobilka, B. K.; Stevens, R. C. *Science* **2007**, *318*, 1258-1265.
(4) Baxter, R. H. G.; Ponomarenko, N.; Å rajer, V.; Pahl, R.; Moffat, K.; Norris, J. R. *P Natl Acad Sci USA* **2004**, *101*, 5982-5987.
(5) Cornaby, S.; Szebenyi, D. M. E.; Smilgies, D.-M.; Schuller, D. J.; Gillilan, R.; Hao, Q.; Bilderback, D. H. *Acta Crystallographica Section D* **2010**, *66*, 2-11.
(6) Ren, Z.; Bourgeois, D.; Helliwell, J. R.; Moffat, K.; Srajer, V.; Stoddard, B. L. *J Synchrotron Radiat* **1999**, *6*, 891-917.
(7) Rhodes, G. *Crystallography Made Crystal Clear - A Guide for Users of Macromolecular Models*; 3rd ed.; Elsevier: Amsterdam, 2006.
(8) Drenth, J. *Principles of Protein X-ray Crystallography*; 3rd ed.; Springer: New York, 2007.

Chapter 4

Concluding remarks

4.1 Summary

In conclusion, a hybrid COC-PDMS, X-ray compatible microfluidic platform was developed which enables the screening and optimization of multiple crystallization conditions and allows *in situ* structure determination of soluble proteins by merging slices of data from different crystals grown on-chip. This involved characterization of COC to ensure that it was suitable for *in situ* analysis. A protocol which would allow fabrication of multilayer COC-PDMS devices was developed and dense pneumatic valve networks were fabricated and tested. A standard goniometer mount was modified to mount these chips on the synchrotron beamlines so as to take advantage of the integrated imaging and sample centering capabilities already in place at the synchrotron. The platform was validated by collecting data from several proteins like lysozyme, thaumatin, ribonuclease A, bacterial defluorinase and bacterial lyase. To get a better understanding of how our approach compares with traditional crystallographic approaches, crystals were grown in traditional microbatch trays, hand mounted on a loop and shot with X-rays under cryogenic conditions. Data was also collected from single lysozyme crystal grown on-chip under cryogenic conditions. The structure of Lysozyme was obtained till 1.55Å by merging datasets from multiple crystals grown on-chip at room temperature. A comparison of crystallographic statistics from these three different approaches shows that our approach compares very well with the data obtained through traditional methods. The array chips developed here can be scaled up very easily and can be modified for different screening experiments, e.g. varying the concentration of the protein and precipitant on-chip. The current platform can be modified and operated using minimal amount of protein in the above configuration.

4.2 Future directions

The current microfluidic platform has been validated for *in situ* structure determination with lysozyme. The next step is to grow novel proteins, which are more difficult to crystallize, on these

platforms and obtain structural information for them. In this regard, two proteins, a novel bacterial lyase and bacterial defluorinase have been crystallized on-chip. Work is ongoing to further optimize the crystal quality and obtain high resolution structural information for these two proteins. The platforms presented here are presently limited to mixing protein and precipitant on-chip. For further work, the design can be modified with additional chambers which can contain a relevant ligand or biomolecule. Flow from these chambers can be driven through valves to expose crystals grown on-chip to these molecules and their effect on the crystal structure can be studied. Stimuli in terms of a pH gradient or light can also be incorporated into the design for further dynamic studies.

The work presented here focuses on the crystallization of soluble proteins. Membrane proteins play an important role in many critical biological processes like cell-cell signaling, material and energy transduction across cellular membranes and immune response and interaction between intra and extra cellular environment. The malfunction of membrane proteins have been linked to several diseases. It is estimated that 60% of current drugs targets are membrane proteins. However, crystallization of membrane proteins is extremely challenging because of the amphiphilic nature and their limited availability.[1,2] The severity of the problem can be gauged from the fact that out of 67,000 structures in the Protein Data Bank[3] less than 1% are membrane proteins and just 15 are human membrane proteins.[4-6] One of the approaches to crystallize membrane proteins is *in meso* crystallization[7], which has shown great promise in crystallizing many novel membrane proteins. This approach involves mixing protein solution with a lipid to form an extremely viscous lipidic cubic phase. A microfluidic platform to generate these cubic phases using an on-chip lipid mixer has been demonstrated.[8] However *in situ* crystallography of lipidic cubic phase in a microfluidic platform with active fluid control has not been shown yet. Having demonstrated that a hybrid COC-PDMS chip is suitable of *in situ* analysis, the next step would be to implement the lipid mixer in an X-ray transparent device. This would enable not only structure determination of membrane proteins but also facilitate dynamic crystallographic studies on membrane proteins.

4.3 References

(1) Nollert, P.; Navarro, J.; Landau, E. M. *Method Enzymol* **2002**, *343*, 183-199.
(2) Gabrielsen, M.; Gardiner, A. T.; Fromme, P.; Cogdell, R. J. In *Current Topics in Membranes, Volume 63*; Volume 63 ed.; DeLucas, L., Ed.; Academic Press: 2009, p 127-149.

(3) RCSB Protein Data Bank. http://www/rcsb.org
(4) Arinaminpathy, Y.; Khurana, E.; Engelman, D. M.; Gerstein, M. B. *Drug Discovery Today*, *In Press, Corrected Proof*.
(5) Dauter, Z.; Lamzin, V. S.; Wilson, K. S. *Current Opinion in Structural Biology* **1997**, *7*, 681-688.
(6) Membrane Proteins of known 3D structure. http://www.blanco.biomol.uci.edu/Membrane_Proteins_xtal.html
(7) Landau, E. M.; Rosenbusch, J. P. *P Natl Acad Sci USA* **1996**, *93*, 14532-14535.
(8) Perry, S. L.; Roberts, G. W.; Tice, J. D.; Gennis, R. B.; Kenis, P. J. A. *Cryst Growth Des* **2009**, *9*, 2566-2569.